



Article

Effects of Titanium–Silica Oxide on Degradation Behavior and Antimicrobial Activity of Poly (Lactic Acid) Composites

Arpaporn Teamsinsungvon ^{1,2,3} , Chaiwat Ruksakulpiwat ^{1,2,3} and Yupaporn Ruksakulpiwat ^{1,2,3,*} 

¹ School of Polymer Engineering, Institute of Engineering, Suranaree University of Technology, Nakhon Ratchasima 30000, Thailand

² Center of Excellence on Petrochemical and Materials Technology, Chulalongkorn University, Bangkok 10330, Thailand

³ Research Center for Biocomposite Materials for Medical Industry and Agricultural and Food Industry, Nakhon Ratchasima 30000, Thailand

* Correspondence: yupa@sut.ac.th; Tel.: +66-44-22-3033

Abstract: A mixed oxide of titania–silica oxides (Ti_xSi_y oxides) was successfully prepared via the sol-gel technique from our previous work. The use of Ti_xSi_y oxides to improve the mechanical properties, photocatalytic efficiency, antibacterial property, permeability tests, and biodegradability of polylactic acid (PLA) was demonstrated in this study. The influence of different types and contents of Ti_xSi_y oxides on crystallization behavior, mechanical properties, thermal properties, and morphological properties was presented. In addition, the effect of using Ti_xSi_y oxides as a filler in PLA composites on these properties was compared with the use of titanium dioxide (TiO_2), silicon dioxide (SiO_2), and TiO_2SiO_2 . Among the prepared biocomposite films, the PLA/ Ti_xSi_y films showed an improvement in the tensile strength and Young's modulus (up to 5% and 31%, respectively) in comparison to neat PLA films. Photocatalytic efficiency to degrade methylene blue (MB), hydrolytic degradation, and in vitro degradation of PLA are significantly improved with the addition of Ti_xSi_y oxides. Furthermore, PLA with the addition of Ti_xSi_y oxides exhibited an excellent antibacterial effect on Gram-negative bacteria (*Escherichia coli* or *E. coli*) and Gram-positive bacteria (*Staphylococcus aureus* or *S. aureus*), indicating the improved antimicrobial effectiveness of PLA composites. Importantly, up to 5% Ti_xSi_y loading could promote more PLA degradation via the water absorption ability of mixed oxides. According to the research results, the PLA composite films produced with Ti_xSi_y oxide were transparent, capable of screening UV radiation, and exhibited superior antibacterial efficacy, making them an excellent food packaging material.

Keywords: titanium silicon oxide; hydrolytic degradation; titania; silica; antimicrobial activity; photocatalytic degradation



Citation: Teamsinsungvon, A.; Ruksakulpiwat, C.; Ruksakulpiwat, Y. Effects of Titanium–Silica Oxide on Degradation Behavior and Antimicrobial Activity of Poly (Lactic Acid) Composites. *Polymers* **2022**, *14*, 3310. <https://doi.org/10.3390/polym14163310>

Academic Editors: Alexandre Vetcher and Alexey Iordanskii

Received: 18 July 2022

Accepted: 11 August 2022

Published: 14 August 2022

Publisher's Note: MDPI stays neutral with regard to jurisdictional claims in published maps and institutional affiliations.



Copyright: © 2022 by the authors. Licensee MDPI, Basel, Switzerland. This article is an open access article distributed under the terms and conditions of the Creative Commons Attribution (CC BY) license (<https://creativecommons.org/licenses/by/4.0/>).

1. Introduction

Higher usage rates of plastics all over the world are causing an increasing rate of disposal of this petroleum-based product. In addition, the limited obtainability of petrochemical resources has become a major global concern [1,2]. Poly (lactic acid) (PLA) is one of the most important biocompatible and biodegradable polymers, and it is a sustainable alternative to petrochemical-derived products [3]. PLA is a synthetic biodegradable polymer, made up of a repeated monomer unit: lactic acid (LA). It is derived from renewable and degradable resources such as corn and rice, and decomposes through simple hydrolysis into water and carbon dioxide. PLA has been viewed as one of the most promising materials because of its excellent biodegradability, biocompatibility, composability, renewability, transparency, high strength, and high modulus [4,5]. Moreover, PLA degradation products are non-toxic (at a lower composition) making it a natural choice for biomedical applications [5,6]. Therefore, this polymer has attracted a wide range of attention in various

applications. However, PLA has a slow degradation rate and hydrophobicity, so it does not decompose fast enough for industrial decomposers [7–9].

To overcome such shortcoming, extra materials are added to fulfill the essential properties such as improved mechanical, heat stability, and barrier properties, and controlled degradation. In addition, the critical hydrolytic degradation rate often limits its application. The rate of degradation could be controlled by adding plasticizers and additives [10]. Although PLA can be degraded with microorganisms in the ground, it takes over two months to decompose, and does not degrade in air [11]. One method to solve this drawback is to add photodegradability filler into PLA, which helps improve degradability under any conditions [12].

Numerous modifications such as copolymerization, plasticization, polymer blends, and polymer composites have been applied to improve some PLA properties. An example of such modifications is to incorporate nanoparticles into the PLA matrix to enhance PLA properties and control the degradation process in various media [13]. The addition of selected nanofillers into PLA, such as organomodified layered silicates (OMLS) [14], carbon nanotubes (CNTs) [15], zinc oxide [16], silica nanofillers (SiO_2) [17,18], and titanium dioxide (TiO_2) [19], can enhance PLA's characteristic features. However, among the nanofillers mentioned above, TiO_2 is the most widely used. TiO_2 or titania is well recognized as a valuable material used in applications such as paints or filler in paper, polymers, textiles, photocatalysis, etc. Nano- TiO_2 particles hold many good properties such as good chemical resistance, high chemical stability [20], attractive photocatalytic activity, excellent photostability, biocompatibility, and antimicrobial activity [21]. Another most-popular nanofiller is silicon dioxide (SiO_2) or silica, a chemical compound that contains oxygen and silicon. Within inorganic oxide fillers, SiO_2 admits much concentration because of its well-defined ordered structure, the easy surface modification, high surface area, and cost-effective production [22]. SiO_2 helps improve the strength, modulus of elasticity, wear resistance, heat and fire resistances, and insulation of properties of polymer materials [23]. Moreover, SiO_2 has been widely applied in food additives, drug delivery, bioimaging, gene delivery, and engineering. Additionally, SiO_2 is classified by the FDA as a “generally regarded as safe” (GRAS) agent, thus making it an ultimate candidate for biomedical applications [24]. The binary oxides are prepared for many purposes: to expand the chemical properties, to develop specific textural properties, or to produce a particle with a personalized composition that is known to present unique characteristics (large surface areas, thermal stability, etc.) [25].

Furthermore, the antimicrobial activity of PLA is usually obtained by adding several metal particles and metal oxides such as silver (Ag) particles [26], zinc oxide (ZnO) [27,28], titanium dioxide (TiO_2) [29,30], and magnesium oxide (MgO) [31] as antibacterial agents.

The objective of the present research was to study PLA composites incorporated with Ti_xSi_y oxide of different concentrations in PLA. We have inspected the influence of TiO_2 , SiO_2 , and Ti_xSi_y oxide on the mechanical properties, thermal properties, morphological properties, and degradation of PLA in various media. In addition, the antimicrobial activity of the PLA composite was investigated. Furthermore, the addition of $\text{Ti}_{70}\text{Si}_{30}$ oxides into PLA significantly improved the photocatalytic efficiency of degrading methylene blue (MB), hydrolytic degradation, and the in vitro degradation of PLA. In addition, PLA, with the addition of $\text{Ti}_{70}\text{Si}_{30}$ oxides, exhibited an excellent antibacterial effect on Gram-negative bacteria (*E. coli*) and Gram-positive bacteria (*S. aureus*), indicating the improved antimicrobial effectiveness of PLA composites. As a result, $\text{Ti}_{70}\text{Si}_{30}$ oxide was used to study the influence of the contents of Ti_xSi_y oxides on the mechanical properties, thermal properties, morphological properties, and degradation of PLA in various media, and the antimicrobial activity of PLA.

2. Materials and Methods

2.1. Materials

Poly (lactic acid) (PLA, grade 4043D) was supplied from Nature Works LLC (Minnetonka, MN, USA), a commercial grade for 3D printing and film applications. Tetraethy-

lorthosilicate (TEOS, 98%, AR grade) and Titanium (IV) isopropoxide (TTIP, 98%, AR grade) were purchased from Acros (Geel, Belgium). Absolute ethanol (C₂H₅OH, AR grade), hydrochloric acid (HCl, AR grade), and ammonium hydroxide (NH₄OH, AR grade) were supplied from Carlo Erba Reagents (Emmendingen, Germany). TiO₂, SiO₂, and Ti_xSi_y oxide prepared in-house were used as filler [32,33]. Particle size of SiO₂, Ti₇₀Si₃₀, Ti₅₀Si₅₀, and Ti₄₀Si₆₀ oxide used in this study were in the range of 130–150 nm. TiO₂ can be generally synthesized under high acid conditions to obtain a uniform spherical shape and small nanoparticles in the range of 25–50 nm [34]. However, the author could synthesise Ti_xSi_y under alkali conditions to control hydrolysis step of Ti-precursor to obtain a uniform shape and size in the range of 130–150 nm because Ti-precursor decreased the reactivity of the alkoxide, hence low concentration of Ti-precursor decreased reactivity of the alkoxide with the lower hydrolysis rate [35].

2.2. Preparation of PLA Composite Films

PLA and PLA composites were prepared by solvent film casting method. First, Ti₇₀Si₃₀, Ti₅₀Si₅₀, Ti₄₀Si₆₀, SiO₂, and TiO₂ were dispersed in chloroform with ultrasonic treatment for 1 day. After that, PLA was added to the Ti_xSi_y oxide and strictly stirred for 4 days. The dispersions of PLA composites were additionally ultrasonically treated for 1 h with frequency of 42 kHz for four times per day. Then, the treated dispersions were slightly poured onto Petri dishes, and the solvent was evaporated under room temperature. The films were dried to constant mass at room temperature for ~24 h and stored in oven at 40 °C for 4 h. Pure PLA and PLA composite films had uniform thickness of 250 ± 4.68 µm. After that, Ti_xSi_y oxides were synthesized using a modified Stöber method involving simultaneous hydrolysis and condensation of TEOS, and Ti_xSi_y mixed oxides' preparation was reported in details in Teamsinsungvon et al. [32].

2.3. Mechanical Properties

The tensile properties of PLA and PLA composites films were obtained in accordance with the ASTM standard method D882-18 using an Instron universal testing machine (UTM, model 5565, Norwood, MA, USA) with a load cell of 5 kN. Specimen samples were 10 cm × 2.54 cm. Crosshead speed was set at 50 cm/min. The values were presented as the average of seven measurements.

2.4. Thermal Properties

Thermal properties of PLA and PLA composites films were carried out using a differential scanning calorimeter (DSC204F1, Netzsch, Selb, Germany) equipped with a liquid nitrogen cooling system. The samples were heated from room temperature to 180 °C with a heating rate of 5 °C/min (1st heating scan) and stored for 5 min to erase previous thermal history. Then it was cooled to room temperature (25 °C) with a cooling rate of 5 °C/min. Finally, it was heated again to 180 °C with heating rate 5 °C/min (2nd heating scan). The degree of crystallinity (X_c) of PLA and PLA composites was estimated using Equation (1) [36,37]:

$$X_c = \frac{\Delta H_m}{\Delta H_m^0 \cdot (\phi_{PLA})} \cdot 100 \quad (1)$$

where ΔH_m are the melting enthalpy in the second heating process, ΔH_m^0 , which is the melting enthalpy of an infinitely large crystal, was taken as 93.6 J/g [38], and ϕ_{PLA} is the PLA weight fraction in the composites.

Thermogravimetric analysis of PLA and PLA composite films were examined using thermogravimetric analyzer (TGA/DSC1, Mettler Toledo, Columbus, OH, USA). The temperature was raised from the room temperature to 650 °C under nitrogen and then heated to 800 °C under air atmosphere at heating rate of 10 °C/min. The weight change was recorded as a function of temperature.

2.5. Morphological Properties

Morphological properties of the film were examined through a scanning electron microscope (JEOL, JSM-6010LV, Tokyo, Japan). An EDAX Genesis 2000 energy dispersive spectrometer (AMETEK, Inc., Berwyn, PA, USA) was applied to determine the spatial distribution of Ti and Si in PLA composite. SEM images of the samples were collected using acceleration voltage 9–12 kV. The cross-sections of the films after tensile test and the freeze-fractured films in liquid nitrogen were sputtered with gold.

2.6. Water Vapor Transmission Rate (WVTR)

WVTR, a modified ASTM standard method E96, is a measure of the rate of water that passes through PLA and its composites film at a particular time interval. To analyze, the composite films were cut into circular discs of 1.5 cm diameter and placed on the top of the glass vial containing 5 mL water. Constant humidity was maintained by placing it in the desiccators maintained at room temperature and relative vapor pressure (RVP) = 0 by using silica gel. The vial assembly was weighted every hour on first day, and then the weighting was performed daily over a 20-day period. In terms of statistical approach, when the straight line adequately fit the weight change vs. time plot using linear regression with $r^2 \geq 0.99$, the constant rate of weight change was obtained. WVTR was calculated using the Equation (2) [39,40]. WVTR ($\text{g m}^{-2} \text{day}^{-1}$) for each type of film was determined using three individually prepared films as the replicated experimental units.

$$WVTR = \frac{G}{t \cdot A} \quad (2)$$

where G = weight change of the vial with water and film (from the straight line) (g), T = the duration for the measurement (day), G/t = slope of the straight line (g day^{-1}), and A = the test area of the film (m^2).

2.7. Photocatalytic Degradation of Methylene Blue (MB)

The photocatalytic activity of PLA composite films was evaluated by degrading methylene blue (MB) under UV light according to Chinese standard GB/T 23762-2009. Specimens of pure PLA and PLA composite films were $5 \text{ cm} \times 15 \text{ cm}$. Five pre-wetted film of each pure PLA and PLA composite films were placed in a flask, then 200 mL of MB solution (10 mg/L) was added. The flask was placed on a mechanical shaker at 50 rpm in a UV chamber with 4 UV lamps (LP Hg lamps, 8 watts, main light emission at 245 nm). The 4 mL MB solution was collected every 60 min, and analyzed using UV-vis spectrophotometer (Cary300, Agilent Technology, Santa Clara, CA, USA). To maintain the volume of solution in the flask, the samples were placed back after each measurement. The maximum absorbance of MB occurs at 664 nm (Figure 1a). The spectrometer was calibrated with solution of MB at 1 mg/L, 3 mg/L, 5 mg/L, 7 mg/L, and 10 mg/L concentrations, respectively. Calibration curve of methylene blue aqueous solutions are shown in Figure 1b. The samples and the solution were stored in a black box to correct the possible decompositions of MB under UV light in absence of any photocatalyst. The concentration of MB was also measured every 60 min to evaluate the absorption of MB. The values were presented as the average of five measurements.

2.8. Light Transmittance and Opacity Measurements

The UV-vis transmission spectra of the film specimens were recorded in the range of 200–800 nm using a UV-vis spectrophotometer (Cary300, Agilent Technology, Santa Clara, CA, USA), according to a modified standard procedure of the British Standards Institution (BSI 1968). The film specimens were directly placed in cells, and empty cells were used

as reference. The opacity of the film specimens was determined with well-controlled thicknesses. Equation (3) was used to calculate the *Opacity* ($\text{AU}\cdot\text{nm}\cdot\text{mm}^{-1}$) of the films:

$$\text{Opacity} = \frac{\text{Abs}_{600}}{b} \quad (3)$$

where Abs_{600} = the absorbance at 600 nm; the transmittance values were converted to absorbance values using the Lambert–Beer equation and b = the film thickness (mm). This test was triplicated for each type of film [41].

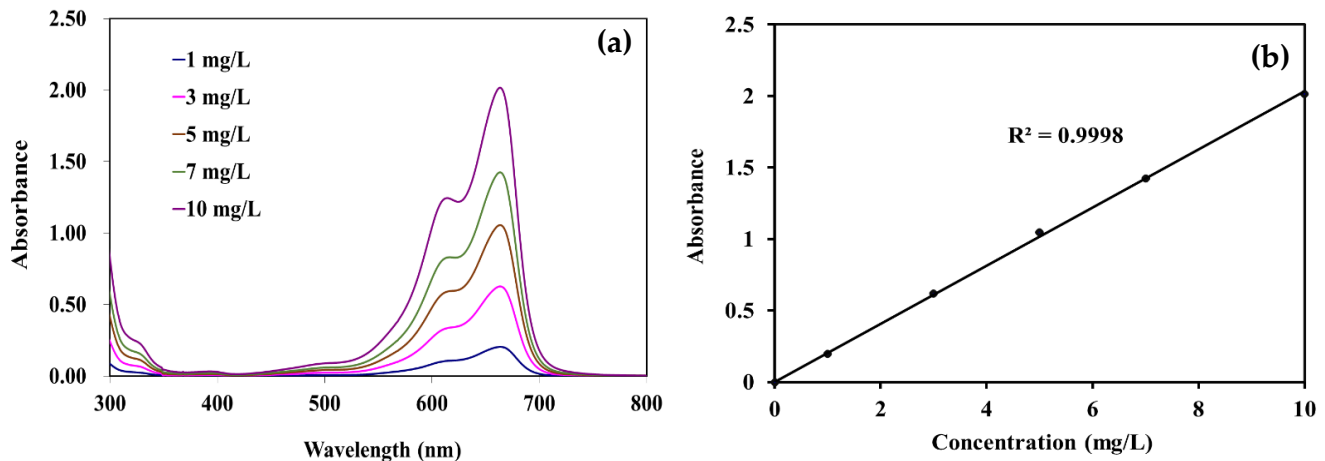


Figure 1. (a) Wavelength–absorbance curves and (b) calibration curve of methylene blue aqueous solutions.

2.9. Hydrolytic Degradation

Hydrolytic degradation of PLA and PLA composite films ($10 \times 10 \text{ mm}^2$) were carried out at 37°C in small bottles containing $1 \text{ mol}\cdot\text{dm}^{-3}$ NaOH solutions (pH 13). Following the incubation for a given time (0, 60, 120, 180, 240, 300, 360, and 420 min), the films were periodically removed, washed with distilled water, and dried in oven at 40°C for 48 h. The weight loss (W_{loss}) was estimated using following Equation (4):

$$W_{\text{loss}}(\%) = \frac{W_0 - W_t}{W_0} \cdot 100 \quad (4)$$

where W_0 = the initial weight of polymer film, and W_t = the weight of degraded sample measured at time t after drying in oven for 48 h [12].

2.10. In Vitro Degradation

The study of degradation of PLA and its composite was carried out following the standards specified by BS EN ISO 10993-13:2010 [42] and ASTM F1635-11 [43]. Each of PLA and PLA composite samples of (0.4–0.5 g) was accurately weighed. The samples were then immersed separately in 0.01 M phosphate-buffered saline (PBS) ($\text{pH} = 7.4 \pm 0.2$) solution and maintained at 37°C with different soaking times from 1 to 8 weeks (0, 2, 4, 6, 8). At various time points, the specimens were washed with deionized water to remove the salts, then oven dried at 40°C for 48 h. Later, dry weights of the samples were recorded. The percentage mass change was determined using the following Equation (5);

$$W_{\text{loss}}(\%) = \frac{W_t - W_0}{W_0} \cdot 100 \quad (5)$$

where W_t = mass of degraded sample measured at time t after drying at 40°C in oven for 48 h, and W_0 = the initial mass of the sample. At each time point, every sample was weighed and mechanically tested, allowing the degradation pathway of each individual sample to be followed with time.

The tensile properties of each specimen were measured by an Instron universal testing machine (UTM, model 5565) with a load cell of 5 kN and crosshead speed of 50 cm/min. The values were presented as the average of five measurements.

2.11. Antimicrobial Activity

Antimicrobial effects of the different samples were determined using the JIS Z 2801:2006 method. The ability of PLA and PLA composite films to restrain the growth of *Escherichia coli* and *Staphylococcus aureus* were investigated. The bacteria were incubated at 37 °C for 24 h. A plate containing a test sample was inoculated with 0.2 mL of an overnight culture of *Escherichia coli* and *Staphylococcus aureus*, while bacterial culture concentration was adjusted to 10⁶ CFU/mL. All petri dishes were incubated at 37 °C for 24 h and colony-forming units (CFU) were counted. Percentage reduction of the colonies was calculated using Equations (6) and (7) below, which relates the number of colonies of neat PLA with that of the composites.

$$\% \text{ Reduction} = \frac{(\text{Log CFU at 0 h} - \text{Log CFU at 24 h})}{\text{Log CFU at 0 h}} \cdot 100 \quad (6)$$

$$\text{Antimicrobial activity}(R) = U_t - A_t \quad (7)$$

where U_t = average of CFU per milliliter after inoculation on untreated test pieces after 24 h; A_t = average of CFU per milliliter after inoculation on antibacterial test pieces after 24 h.

3. Results and Discussion

3.1. Mechanical Properties

The tensile properties of PLA and PLA composites with various Ti₇₀Si₃₀ oxide contents and different types of nanoparticles are listed in Table 1.

Table 1. Tensile properties of PLA, PLA/TiO₂, PLA/SiO₂, PLA/Ti_xSi_y, and PLA/TiO₂SiO₂ composites.

Sample	Tensile Strength (MPa)	Elongation at Break (%)	Young's Modulus (GPa)
PLA	33.94 ± 1.38	19.62 ± 8.64	0.98 ± 0.23
97PLA/3TiO ₂	28.22 ± 1.47	18.1 ± 4.24	1.01 ± 0.04
97PLA/3SiO ₂	29.75 ± 1.38	11.8 ± 4.96	1.07 ± 0.10
97PLA/3Ti ₇₀ Si ₃₀	35.64 ± 3.21	11.12 ± 1.81	1.18 ± 0.06
95PLA/5Ti ₇₀ Si ₃₀	32.06 ± 2.29	9.88 ± 2.81	1.01 ± 0.10
97PLA/3Ti ₅₀ Si ₅₀	35.31 ± 2.01	9.61 ± 2.57	1.29 ± 0.12
97PLA/3Ti ₄₀ Si ₆₀	30.67 ± 1.74	22.30 ± 2.53	1.02 ± 0.05
97PLA/3TiO ₂ SiO ₂	29.00 ± 1.42	58.37 ± 5.00	0.96 ± 0.07

The addition of 3 wt.% of Ti₇₀Si₃₀ and Ti₅₀Si₅₀ slightly increased the tensile strength and Young's modulus and decreased the elongation at break of the PLA composite films compared to neat PLA (Figure 2). This may be due to higher interfacial adhesion between the oxide filler and the PLA matrix by the Van der Waals force or induction interactions, which decreased thereafter when adding a mixed oxide content of up to 5 wt.%, however, it was slightly higher than pure PLA. The result could be attributed to the increased filler quantity leading to a weaker filler–matrix interface and the agglomeration of filler particles, which consequently decreases the tensile strength. The Young's modulus of the composites insignificantly varied in correspondence with Ti_xSi_y oxide (Figure 2c). However, elongation at the break decreased with the addition of Ti_xSi_y oxide (Figure 2b) as a result of the addition of a rigid phase in the PLA composite, which contributed to a reduction of the PLA ductility. Nevertheless, the addition of TiO₂SiO₂ and Ti₄₀Si₆₀ in the PLA matrix increased elongation at the break of PLA.

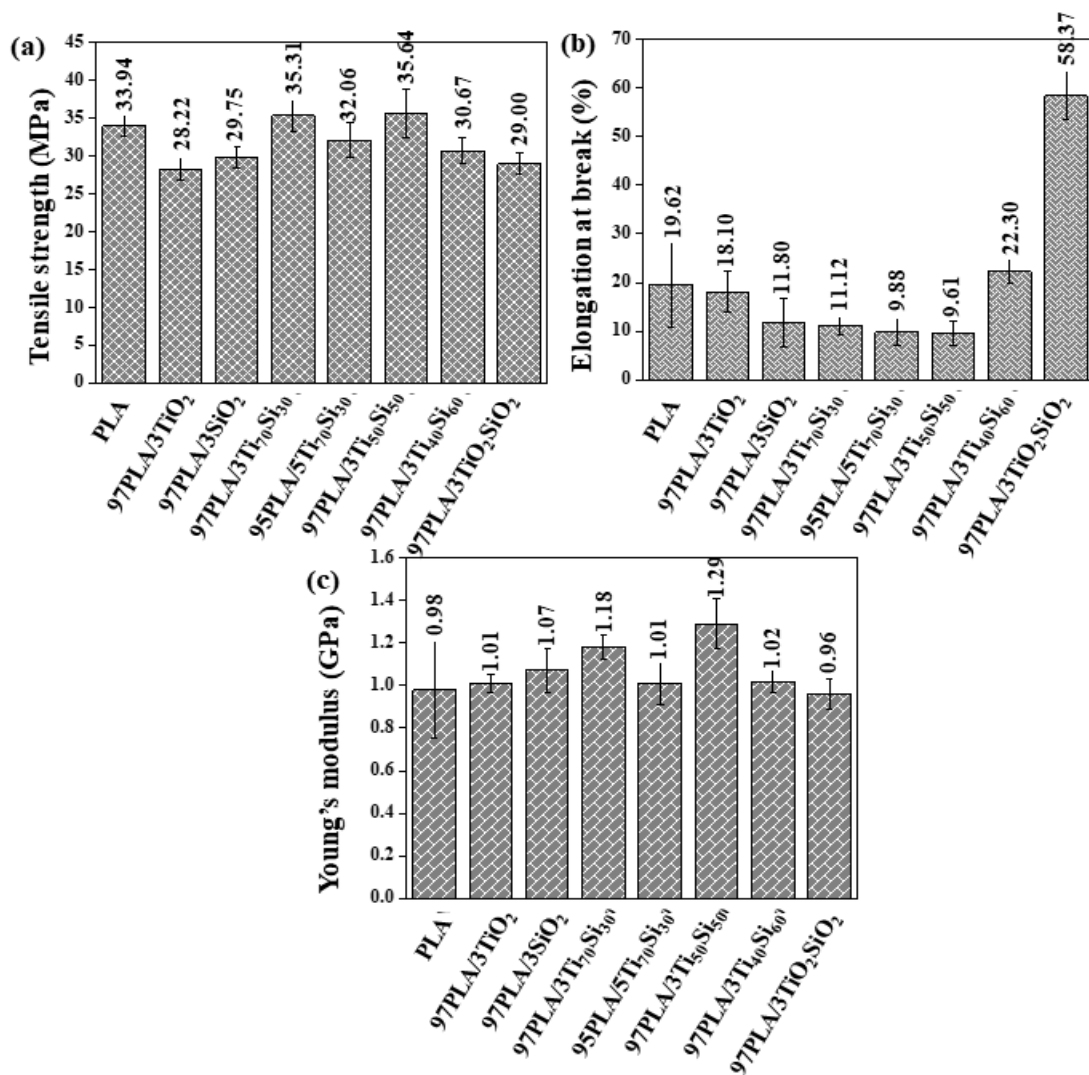


Figure 2. Comparison of the (a) Tensile strength, (b) Elongation at break, and (c) Young's modulus of PLA, PLA/TiO₂, PLA/SiO₂, PLA/Ti_xSi_y, and PLA/TiO₂SiO₂ composites.

During tensile testing, it was observed that the fracture behavior of the film changed for PLA, PLA/TiO₂, PLA/SiO₂, PLA/Ti_xSi_y, and PLA/TiO₂SiO₂ composites. This was demonstrated in the tensile stress–strain curves, as shown in Figure 3. With the addition of filler to the PLA matrix, the composite exhibits elastic behavior, enhancing the toughness of PLA. Furthermore, it was shown that the addition of Ti₇₀Si₃₀ oxide to the PLA polymer matrix resulted in a decrease in the ductile characteristics, while slightly increasing the tensile strength and decreasing elongation at the break. However, the addition of TiO₂SiO₂ and Ti₄₀Si₆₀ oxide increased elongation at the break of PLA. This may be due to the particles of TiO₂SiO₂ in the formulation being homogeneously distributed in the polymer matrix, contributing to the occurrence of plastic deformations in the whole sample, allowing a higher elongation than that of the pure PLA.

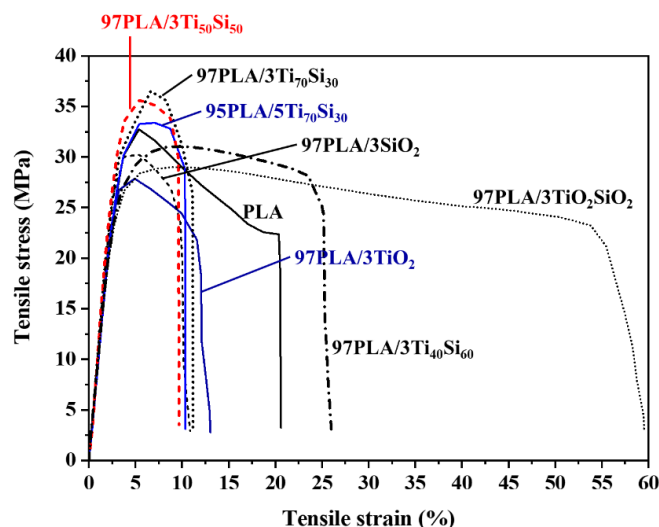


Figure 3. Stress–strain curves of PLA, PLA/TiO₂, PLA/SiO₂, PLA/Ti_xSi_y, and PLA/TiO₂SiO₂ composites.

3.2. Thermal Properties

Thermal behaviors of pure PLA and PLA composites with TiO₂, SiO₂, Ti₇₀Si₃₀, Ti₅₀Si₅₀, Ti₄₀Si₆₀, and TiO₂SiO₂ were investigated using differential scanning calorimetry (DSC), in which first heating scans (1st heating scans), cooling scans, and second heating scans (2nd heating scans) of PLA and PLA composites were performed. DSC thermograms of PLA and PLA composites are shown in Figure 4. The thermal properties of all samples are listed in Table 2. The glass transition temperature (T_g), cold crystallization temperature (T_{cc}), and melting temperature (T_m) of the PLA composites were observed.

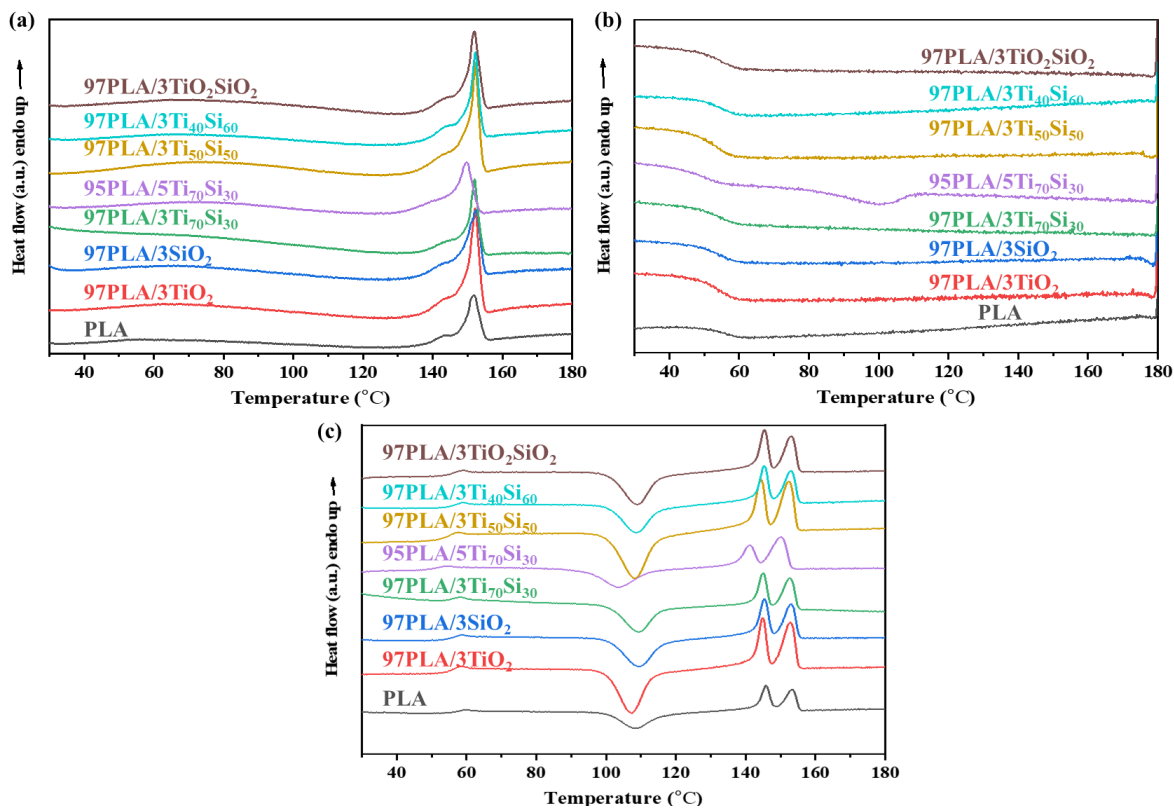


Figure 4. DSC thermogram of (a) first heating, heating rate 5 °C/min, (b) cooling, cooling rate 5 °C/min, (c) second heating, heating rate 5 °C/min of PLA, PLA/TiO₂, PLA/SiO₂, PLA/Ti_xSi_y, and PLA/TiO₂SiO₂ composites.

Table 2. Thermal characteristics of PLA, PLA/TiO₂, PLA/SiO₂, PLA/Ti_xSi_y, and PLA/TiO₂SiO₂ composites (the second heating, heating rate 5 °C/min).

Samples	T _g , °C	T _{cc} , °C	ΔH _c , J/g	T _{m1} , °C	T _{m2} , °C	ΔH _m , J/g	χ _c , %
PLA	58.87	109.47	36.15	145.84	153.35	31.73	33.86
97PLA/3TiO ₂	56.86	107.36	33.61	144.89	152.72	33.17	36.50
97PLA/3SiO ₂	56.64	108.22	33.06	145.39	145.33	33.31	36.65
97PLA/3Ti ₇₀ Si ₃₀	54.81	107.3	34.41	145.07	152.75	32.71	35.99
95PLA/5Ti ₇₀ Si ₃₀	51.84	103.09	26.80	141.29	150.22	32.18	36.15
97PLA/3Ti ₅₀ Si ₅₀	55.96	107.14	33.06	144.41	152.50	34.44	37.89
97PLA/3Ti ₄₀ Si ₆₀	57.40	107.72	34.16	145.33	153.01	33.38	36.73
97PLA/3TiO ₂ SiO ₂	57.46	107.79	30.54	145.39	153.07	32.31	35.55

T_g and T_{cc} of neat PLA occur at 58.87 °C and 109.47 °C, respectively, while T_m appeared at 145.84 °C and 152.35 °C, respectively. The double melting endotherms of neat PLA were explained by the melting and recrystallization. The peak at a low temperature was attributed to the melting of the crystals formed during the non-isothermal melt crystallization, while the peak at a high temperature corresponded to the re-melting of the newly-formed crystallite during melting, and recrystallization during the DSC heating scans [44]. However, T_c of the neat PLA did not appear in the cooling cycle. The addition of TiO₂, SiO₂, Ti₇₀Si₃₀, Ti₅₀Si₅₀, Ti₄₀Si₆₀, and TiO₂SiO₂ in the PLA matrix showed insignificant effects on the glass transition temp (T_g), cold crystallization temp (T_{cc}), and melting temp (T_m) of PLA. After the cooling scan (Figure 4b), no crystallization temperatures (T_c) were observed in all composites in the cooling cycle. However, by adding 5wt.% of Ti₇₀Si₃₀ oxide into PLA, T_c was only observed at 101 °C when cooling the sample in the DSC measurement at a cooling rate of 5 °C/min.

Cold crystallization is a phenomena that occurs from re-crystallization during the heating process of polymers [45]. Cold crystallization behaviors (Figure 4c) of PLA films containing 3 wt.% of TiO₂, SiO₂, Ti₇₀Si₃₀, Ti₅₀Si₅₀, Ti₄₀Si₆₀, and TiO₂SiO₂ nanoparticles and 5 wt.% of Ti₇₀Si₃₀ were observed. For neat PLA, there is a slightly cold crystallization peak around 109.47 °C. While adding 3 wt.% of TiO₂, SiO₂, Ti₇₀Si₃₀, Ti₅₀Si₅₀, Ti₄₀Si₆₀, and TiO₂SiO₂ into PLA, the cold crystallization peak of PLA composites shifted to a lower temperature by approximately 1–2 °C. Moreover, the T_{cc} of the PLA composite shifted to 103.09 °C with Ti₇₀Si₃₀-loading rising to 5 wt.%, showing that a 5 wt.% Ti₇₀Si₃₀ addition can promote PLA crystallization. This might be attributed to the increase of the chain mobility of PLA, and the Ti_xSi_y oxide could act as an efficient cold crystal nuclei site, which consequently increased the crystallinity of PLA. These results suggest that Ti₇₀Si₃₀ oxide had a positive effect on the promotion of the crystallization of PLA and could act as a nucleating agent. Similar to other results, Chen et al. [45] found that by incorporating a composite nucleating agent (CNA) to PLA, the polymer could decrease T_{cc}, indicating that the crystallization ability of the PLA composite can be enhanced in such a way.

The addition of 5 wt.% Ti₇₀Si₃₀ is found to be able to enhance the T_m of PLA composites. This is possibly a result of the heterogeneous nucleation effects of Ti₇₀Si₃₀ nanoparticles on PLA during the crystallization process. The lamella formation of PLA was hindered by Ti₇₀Si₃₀ and led to less perfect crystals of PLA [46]. While the addition of a 3 wt.% of TiO₂, SiO₂, Ti₇₀Si₃₀, Ti₅₀Si₅₀, Ti₄₀Si₆₀, and TiO₂SiO₂ did not significantly affect the T_m of PLA, the degree of crystallinity (χ_c) of neat PLA significantly increased with incorporating TiO₂, SiO₂, Ti₇₀Si₃₀, Ti₅₀Si₅₀, Ti₄₀Si₆₀, and TiO₂SiO₂, indicating that TiO₂, SiO₂, Ti₇₀Si₃₀, Ti₅₀Si₅₀, Ti₄₀Si₆₀, and TiO₂SiO₂ can act as nucleating agents for PLA.

Thermal degradation at 5% weight loss (T_{0.05}), 50% weight loss (T_{0.5}), final degradation (T_f), and the char formation at 800 °C of PLA and PLA composites are listed in Table 3, respectively. TGA and DTG curves of PLA and PLA composites at a heating rate of 10 °C/min are shown in Figure S1a,b, respectively. The presence of TiO₂, SiO₂, Ti₇₀Si₃₀, Ti₅₀Si₅₀, Ti₄₀Si₆₀, and TiO₂SiO₂ did not change the thermal decomposition behavior of PLA, while the mass loss between 250–365 °C was observed, which corresponded to the

decomposition of PLA. Then from 365 to 600 °C thermal analysis curves slowed down to complete the decomposition of the PLA matrix until a constant mass was reached. The constant mass remaining at the end of each TGA experiment corresponded to amounts of nanoparticles in PLA composites. In this study, the temperature at 5% weight loss ($T_{0.05}$) was defined as the onset degradation temperature for the evaluation of the TiO_2 , SiO_2 , and Ti_xSi_y oxide effects on the thermal stability of the PLA composites.

Table 3. Thermal degradation temperature of PLA, PLA/ TiO_2 , PLA/ SiO_2 , PLA/ Ti_xSi_y , and PLA/ TiO_2SiO_2 composites.

Samples	$T_{0.05}$, °C	$T_{0.5}$, °C	T_d , °C	T_f , °C	Residual, %
PLA	321.67	360.33	358.83	424.64	1.20
97PLA/3 TiO_2	336.17	363.67	363.17	429.22	4.07
97PLA/3 SiO_2	331.17	361.17	359.33	427.27	4.14
97PLA/3 $\text{Ti}_{70}\text{Si}_{30}$	304.00	351.83	350.17	408.68	3.91
95PLA/5 $\text{Ti}_{70}\text{Si}_{30}$	284.50	347.33	346.33	407.16	5.46
97PLA/3 $\text{Ti}_{50}\text{Si}_{50}$	324.50	358.36	356.50	425.49	4.22
97PLA/3 $\text{Ti}_{40}\text{Si}_{60}$	326.50	358.67	356.83	416.83	3.53
97PLA/3 TiO_2SiO_2	330.67	362.33	361.33	418.69	4.50

It is obvious that the T_{onset} of the PLA composites shifted to a higher temperature with the presence of 3 wt.% of TiO_2 , SiO_2 , $\text{Ti}_{50}\text{Si}_{50}$, $\text{Ti}_{40}\text{Si}_{60}$, and TiO_2SiO_2 . Consequently, the thermal stability of the PLA composites was improved. A possible reason to explain this behavior is that TiO_2 , SiO_2 , $\text{Ti}_{50}\text{Si}_{50}$, $\text{Ti}_{40}\text{Si}_{60}$, and TiO_2SiO_2 particles may act as a heat barrier in the early stage of thermal decomposition [12]. Similar data have been reported by Zhang et al., who studied PLA composites obtained by adding TiO_2 to poly (lactic acid) [47]. However, PLA with the addition of 3 wt.% of $\text{Ti}_{70}\text{Si}_{30}$ oxide was found to present a lower onset temperature than that of pure PLA, which resulted in a decrease in the PLA thermal stability. Moreover, it was found that the onset degradation temperature of the composites shifted to a lower temperature with increasing $\text{Ti}_{70}\text{Si}_{30}$ oxide nanoparticles loading from 3 to 5 wt.%. This suggests that there might be degradation due to the water absorption of the filler that would be associated with the cleavage of the chain of PLA at the ester group ($-\text{C}-\text{O}-$) by water molecules due to hydrolysis leading to decreased the thermal stability of PLA.

Moreover, the peak in the DTG curves represented the temperature maximum degradation rate (Figure S1b). PLA/3 TiO_2 exhibited the fastest degradation rate at the highest temperature, compared to neat PLA and other PLA composites. However, the degradation temperature of the PLA/ $\text{Ti}_{70}\text{Si}_{30}$ composite shifted to a lower temperature. This suggested that the thermal stability of PLA decreased with the incorporation of $\text{Ti}_{70}\text{Si}_{30}$ loading. In addition, when 3 wt.% TiO_2 , SiO_2 , $\text{Ti}_{70}\text{Si}_{30}$, $\text{Ti}_{50}\text{Si}_{50}$, $\text{Ti}_{40}\text{Si}_{60}$, and TiO_2SiO_2 , and 5 wt.% $\text{Ti}_{70}\text{Si}_{30}$ mixed oxides were added to PLA, the composites left the char residual of fillers at 4.07, 4.14, 3.91, 4.22, 3.53, 4.50, and 5.46%, respectively, for the PLA composites. The char residual generally depended on the amount of added nanoparticles [48].

3.3. Morphological Properties

In order to investigate the dispersion and distribution of TiO_2 , SiO_2 , $\text{Ti}_{70}\text{Si}_{30}$, $\text{Ti}_{50}\text{Si}_{50}$, $\text{Ti}_{40}\text{Si}_{60}$, and TiO_2SiO_2 in the PLA composites films, SEM analysis was performed. SEM micrographs of the fracture surface of PLA and PLA adding 3 wt.% of TiO_2 , SiO_2 , $\text{Ti}_{70}\text{Si}_{30}$, $\text{Ti}_{50}\text{Si}_{50}$, $\text{Ti}_{40}\text{Si}_{60}$, and TiO_2SiO_2 , and 5 wt.% of $\text{Ti}_{70}\text{Si}_{30}$ are shown in Figure 5a, and the surface of the PLA and PLA composites films after the tensile test is shown in Figure 5b.

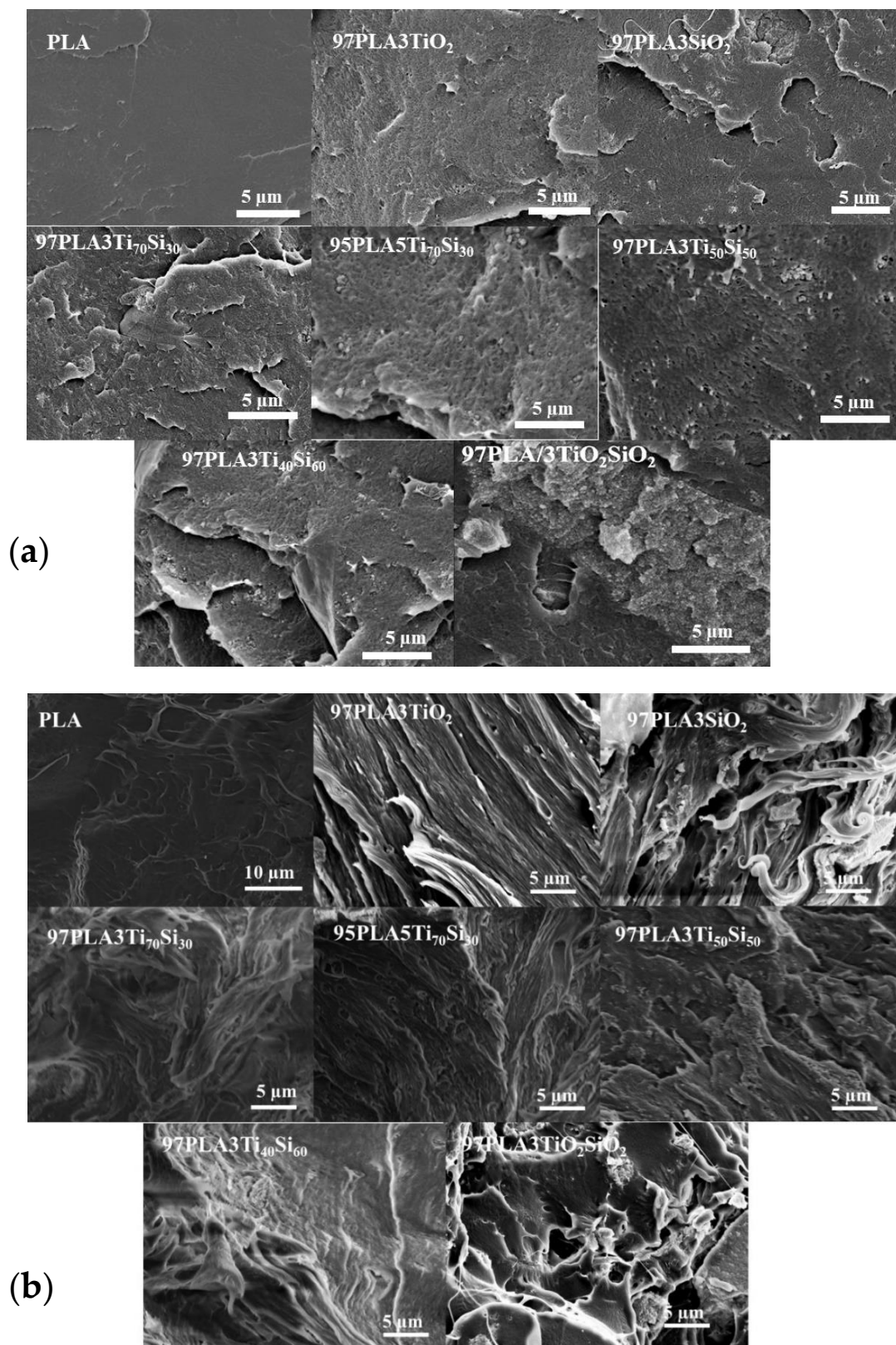


Figure 5. SEM micrographs ($\times 2.5$ k, WD = 13–15 mm, acceleration voltage 9–12 kV) of (a) the fracture surface and (b) after tensile testing of PLA, PLA/TiO₂, PLA/SiO₂, PLA/Ti_xSi_y, and PLA/TiO₂SiO₂ composites.

The SEM results showed that a relatively brittle and comparatively flat surface without holes and air bubbles was found on the fracture surface of the pure PLA films. Meanwhile, SEM images of all PLA composites exhibited roughness caused by adding 3 wt.% of TiO_2 , SiO_2 , $\text{Ti}_{70}\text{Si}_{30}$, $\text{Ti}_{50}\text{Si}_{50}$, $\text{Ti}_{40}\text{Si}_{60}$, and TiO_2SiO_2 nanoparticles, particularly at 3 wt.% of TiO_2SiO_2 (Figure 5a). The enhancement of the mechanical properties depended on the absence of voids, undamaged position of fillers, interfacial bonding between the fillers and matrix, and the absence of an agglomerate of fillers [49]. However, the white spots in the PLA composites micrographs illustrates the agglomerates of TiO_2 , SiO_2 , $\text{Ti}_{70}\text{Si}_{30}$, $\text{Ti}_{50}\text{Si}_{50}$, $\text{Ti}_{40}\text{Si}_{60}$, and TiO_2SiO_2 in the PLA matrix, leading to poor mechanical properties. In this work, although some agglomerations could be observed in all PLA composite films, 3wt.% of $\text{Ti}_{70}\text{Si}_{30}$ and $\text{Ti}_{50}\text{Si}_{50}$ was still kept intact within the PLA matrix (Figure 5b). As $\text{Ti}_{70}\text{Si}_{30}$ -loading was increased to 5 wt.%, the position of $\text{Ti}_{70}\text{Si}_{30}$ in PLA was displaced, leading to the formation of a gap between the filler surface and PLA matrix. Therefore, it is an indication of poor interfacial adhesion between $\text{Ti}_{70}\text{Si}_{30}$ and PLA at high loading [50].

The EDX elemental mapping results (Figure 6b–e) suggested the existence of Ti_xSi_y mixed oxides in the PLA composites. Furthermore, EDX elemental analysis results (Figure 6f) of the selected area also confirmed the spatial distribution of the Si, Ti, and O elements of the Ti_xSi_y mixed oxide in the PLA composite. The distribution of Si and Ti in the particles was relatively uniform in the case of the PLA/3 $\text{Ti}_{70}\text{Si}_{30}$ composite.

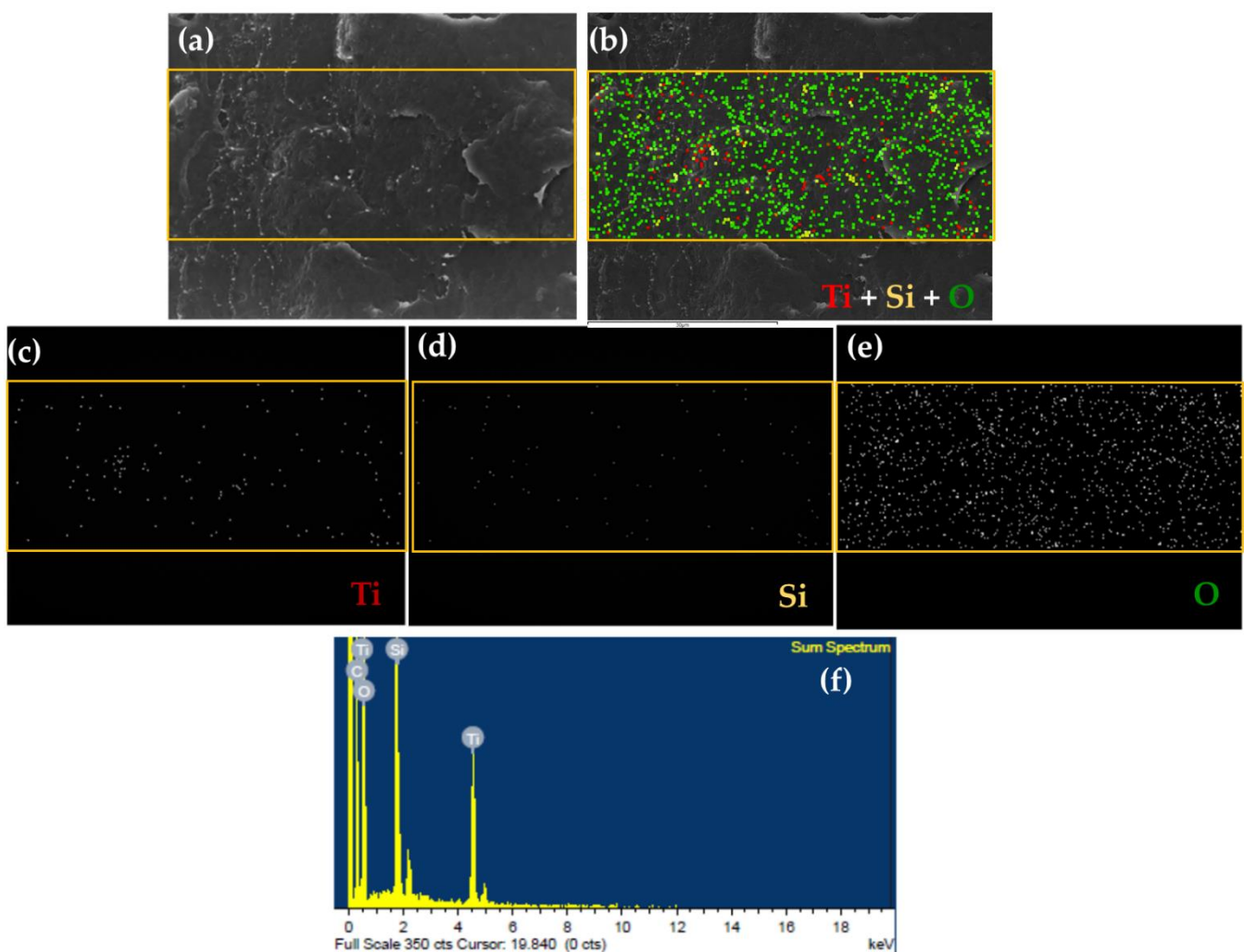


Figure 6. (a) SEM images (b) over all elements in the PLA/ $\text{Ti}_{70}\text{Si}_{30}$ composite and the corresponding elemental mapping analysis of (c) Ti, (d) Si, (e) O, and (f) EDX spectra.

3.4. Water Vapor Transmission Rate (WVTR)

One of the most important properties of bio-based composites films is the ability to evaluate the moisture transfer from the environment to the product. The WVTR of the PLA and PLA composite films is shown in Figure 7. The WVTR of the PLA films was $0.316 \text{ g m}^{-2} \text{ day}^{-1}$ which was lower than the PLA films incorporated with 3wt.% of SiO_2 , $\text{Ti}_70\text{Si}_{30}$, and $\text{Ti}_{50}\text{Si}_{50}$, which were 1.000, 1.023, and $0.523 \text{ g m}^{-2} \text{ day}^{-1}$. In addition, the WVTR of the PLA/ $\text{Ti}_{70}\text{Si}_{30}$ composite film increased with increasing $\text{Ti}_{70}\text{Si}_{30}$ content to 5 wt.%. It is common that, for a solid polymer, the water vapor transmission follows a simple mechanism including adsorbing at the entering face, dissolving, and rapidly creating equilibrium, diffusing through the film, and desorbing at the exit face [51]. The smaller the particle diameter of the nanoparticles is, the more the indirect pathway reducing the diffusion coefficient is produced [52,53]. In other words, the particle diameter is indirectly proportional to the diffusion coefficient. Consequently, the hydrophilicity of the PLA composite incorporating SiO_2 , $\text{Ti}_{70}\text{Si}_{30}$, and $\text{Ti}_{50}\text{Si}_{50}$ was improved.

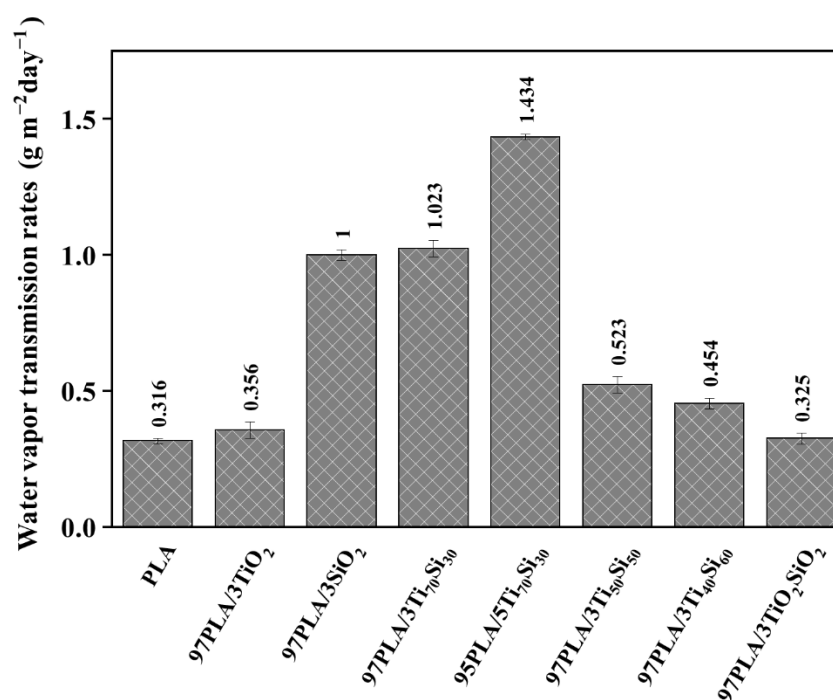


Figure 7. Water vapor transmission rate (WVTR) of PLA, PLA/ TiO_2 , PLA/ SiO_2 , PLA/ Ti_xSi_y , and PLA/ TiO_2SiO_2 composites.

3.5. Photocatalytic Degradation of Methylene Blue (MB)

In this study, the photocatalytic activity of PLA and PLA composite films were investigated by degrading methylene blue (MB). The decomposition of MB might be caused by UV irradiation without the presence of any photocatalyst.

Figure 8 shows changes in the concentration of MB in an aqueous solution under UV irradiation, which was a result of MB decomposition. The presence of 3 wt.% TiO_2 , SiO_2 , $\text{Ti}_{70}\text{Si}_{30}$, $\text{Ti}_{50}\text{Si}_{50}$, $\text{Ti}_{40}\text{Si}_{60}$, and TiO_2SiO_2 in the PLA film matrix exhibited MB degradation more efficiently than using photocatalysis solely. The efficiency to degrade MB was $\text{TiO}_2 > \text{Ti}_{70}\text{Si}_{30} > \text{TiO}_2\text{SiO}_2 > \text{Ti}_{50}\text{Si}_{50} > \text{Ti}_{40}\text{Si}_{60} > \text{SiO}_2$, respectively. It was also found that an increase in $\text{Ti}_{70}\text{Si}_{30}$ -loading to 5wt.% improved the efficiency of the photocatalytic activity of PLA. The photo-activity of the mixed oxide was evidently increased because the high content of the mixed oxide's increasing surface area of the filler effectively concentrated MB around the nanoparticle and produced high concentrations of organic compounds for the photocatalysis, which consequently improved the photocatalytic activity of PLA. It is known that photocatalytic activity occurs at the surface of the photocatalyst. Therefore, the

surface area of PLA composites film, which in turn depends on the size of the nanoparticles, film morphology, and thickness, has an effect on photocatalytic reactivity [54]. The PLA composite film containing TiO_2 can degrade MB more effectively than that containing only photocatalysis. This may be due to two reasons. Firstly, MB was degraded directly by UVC. Secondly, TiO_2 received light energy more than band-gap energy and then the electron in the valence band (VB) was excited to the conduction band (CB), resulting in a generated hole (h^+) (Equation (8)). This hole could oxidize MB (Equation (9)) or oxidized H_2O to produce OH (Equation (10)). The e^- in CB could reduce O_2 at the surface of TiO_2 to generate O_2^- (Equation (11)). The appearance of radical (OH , O_2^-) and h^+ reacted with MB to generate a peroxide derivative and hydroxylate or degrade completely to CO_2 and H_2O [54]. The photodegradation mechanism can be summarized by Equations (8)–(11).

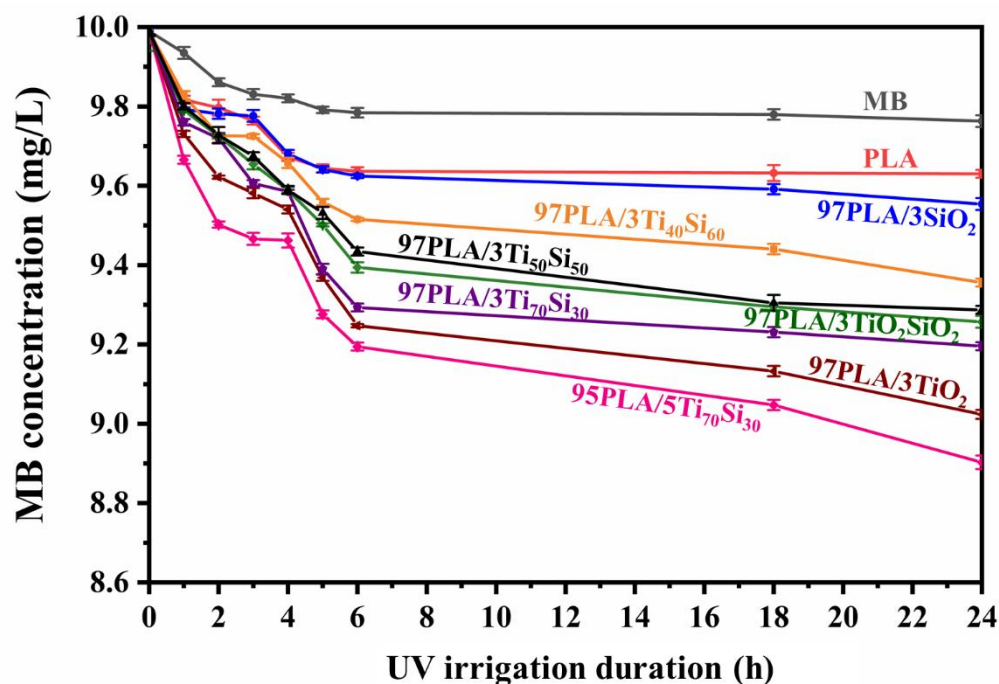


Figure 8. Concentration of methylene blue (MB) due to absorption of PLA, PLA/ TiO_2 , PLA/ SiO_2 , PLA/ Ti_xSi_y , and PLA/ TiO_2SiO_2 composite films under UV irradiation.

The presence of filler in the PLA film matrix shows more efficiency to degrading MB than using only photocatalysis. The enhanced photocatalytic properties of the PLA composites could be mainly attributed to promoted surface adsorption and mass transfer/diffusion, increased light absorption and utilization efficiency, and especially, the higher charge transfer and separation rate by the filler, increased light-harvesting ability, and promoting photoexcitation charge separation, which were the main reasons for improving photocatalytic activity [55,56]. In addition, the photocatalytic activity is influenced by the crystal structure, particle size, specific surface area, and porosity of nanoparticles. So, ultrafine powders of mixed oxide show good catalytic activity. However, agglomeration often takes place, resulting in the reduction or even complete loss of photocatalytic activity.

Due to its photocatalytic activity, $\text{Ti}_{70}\text{Si}_{30}$ nanoparticles with a high specific surface area ($569 \text{ m}^2 \text{ g}^{-1}$) [33] can degrade MB, making it a suitable material for photocatalytic application.

3.6. Light Transmittance and Opacity Measurements

UV light can create free radicals in products by a photochemical reaction, leading to a negative effect for food. Some of the unfriendly effects include the deterioration of antioxidants, destruction to vitamins and proteins, and a change in color. UV radiation is classified into UV-A (wavelength 320–400 nm), UVB (280–320 nm), and UV-C (200–280 nm) [57,58]. For good optical properties, the optical transmittance should exceed 90% in the visible range (measured from 400 to 800 nm). So, the optical transmittance was measured using a light source with a 600 nm wavelength, which is the central wavelength of the visible range. So, a lot of research uses this wavelength to evaluate opacity [41,59,60]. The addition of TiO_2 , SiO_2 , $\text{Ti}_{70}\text{Si}_{30}$, $\text{Ti}_{50}\text{Si}_{50}$, $\text{Ti}_{40}\text{Si}_{60}$, and TiO_2SiO_2 into the PLA matrix caused a significant decrease of transmittance in all UV regions (Table 4). The results show that the addition of filler into the PLA matrix caused a significantly decrease of transmittance in all UV regions. The presence of 3wt.% $\text{Ti}_{70}\text{Si}_{30}$ in the PLA film matrix succeeded in blocking more than 99.6% of the 240, 300, and 360 nm wavelengths, as representatives of UV-C, UV-B, and UV-A radiation, respectively, with a low opacity for the composite film. Moreover, the increase of $\text{Ti}_{70}\text{Si}_{30}$ oxide-loading up to 5wt.% into PLA improved the UV-blocking efficiency.

Table 4. Transmittance (%) and opacity values of PLA, PLA/ TiO_2 , PLA/ SiO_2 , PLA/ Ti_xSi_y , and PLA/ TiO_2SiO_2 composite films in the visible, UV-A, UV-B, and UV-C regions.

Sample	Transmittance, %				Opacity ($\text{AU}\cdot\text{nm}\cdot\text{mm}^{-1}$)
	UV-C (240 nm)	UV-B (300 nm)	UV-A (360 nm)	Visible (600 nm)	
PLA	1.24	24.47	34.77	51.39	1.16
97PLA/3 TiO_2	0.00	0.12	0.41	1.98	6.81
97 PLA/3 SiO_2	0.04	9.48	18.03	38.37	2.31
97 PLA/3 $\text{Ti}_{70}\text{Si}_{30}$	0.00	0.28	0.75	14.00	3.42
95 PLA/5 $\text{Ti}_{70}\text{Si}_{30}$	0.00	0.00	0.36	4.06	6.33
97 PLA/3 $\text{Ti}_{50}\text{Si}_{50}$	0.00	0.32	2.37	15.65	3.22
97 PLA/3 $\text{Ti}_{40}\text{Si}_{60}$	0.00	0.03	0.81	10.48	3.92
97 PLA/3 TiO_2SiO_2	0.00	0.19	1.43	7.30	4.74

The PLA films were transparent and colorless, and the addition of SiO_2 to PLA remained transparent, while other PLA composite films showed higher opacity than the pure PLA film. However, the transparency changes related to the increasing $\text{Ti}_{70}\text{Si}_{30}$ oxide contents from 3 up to 5 wt.% provided totally opaque films by more than two orders of magnitude in the opacity films, but this was still lower than the composite film of PLA with TiO_2 . Similarly, the addition of TiO_2 and $\text{Ti}_{70}\text{Si}_{30}$ made the PLA composites' color appear whiter because of the characteristic whiteness of the TiO_2 and $\text{Ti}_{70}\text{Si}_{30}$ nanoparticles. Photographs of PLA, PLA/ TiO_2 , PLA/ SiO_2 , PLA/ Ti_xSi_y , and PLA/ TiO_2SiO_2 composite films are shown in Figure 9. These results suggest that the PLA composite produced with $\text{Ti}_{70}\text{Si}_{30}$ oxide was suitably applied to transparency packaging with good UV-blocking efficiency.



Figure 9. Photographs of films prepared from PLA, PLA/TiO₂, PLA/SiO₂, PLA/Ti_xSi_y, and PLA/TiO₂SiO₂ composites ($250 \pm 4.68 \mu\text{m}$ thickness).

3.7. Hydrolytic Degradation

Figure 10 shows the percentage weight loss of PLA and PLA composite films as a function of hydrolytic degradation time. Complete degradation of PLA was achieved at about 1200 min, while all of the PLA composite films were hydrolyzed faster than neat PLA. Interestingly, the incorporation of 3 wt.% of TiO₂, SiO₂, Ti₇₀Si₃₀, Ti₅₀Si₅₀, Ti₄₀Si₆₀, and TiO₂SiO₂ exhibited a much higher weight loss as a function of time than neat PLA. The presence of filler induced a much more apparent change of weight loss of hydrolytic degradation, which indicates the enhancement of a hydrolytic degradation ability of the PLA matrix. This was attributed by the addition of nanoparticles, which helped accelerate the hydrolytic degradation of the PLA matrix. Furthermore, 97PLA/3TiO₂, 97PLA/3SiO₂, 97PLA/3Ti₇₀Si₃₀, 97PLA/3Ti₅₀Si₅₀, 97PLA/3Ti₄₀Si₆₀, and 97PLA/3TiO₂SiO₂ were fully degraded at 840, 300, 420, 420, and 560 min, respectively. Moreover, the PLA composite containing 5 wt.% of Ti₇₀Si₃₀ degraded faster than all the composites and it was fully degraded in approximately 240 min. Consequently, it could be concluded that the rate of the hydrolytic degradation of PLA composite films can be controlled by the filler content. This result is in agreement with Buzarovka and Grozdanov (2012) [12].

3.8. In Vitro Degradation

The degradation of PLA in PLA composites involves several processes such as water uptake, ester cleavage and formation if there are oligomer fragments, the dissolution of the oligomer fragment, etc., [61]; as a result, factors affecting the hydrolysis tendency of PLA would control the degradation of PLA. The long-term hydrolytic degradation of PLA and PLA composite films in a phosphate buffered saline (PBS) ($\text{pH} = 7.4 \pm 0.2$) solution at 37 °C was evaluated by mass loss in 56 days. Figure 11 illustrates the mass loss of the PLA and PLA composite with the degradation time. From 0 to 14 days, all of the samples exhibited a dramatic increase in mass loss with increasing immersion time. After this period, the mass loss of all samples accelerated gradually. PLA incorporating with 3 wt.% of TiO₂, SiO₂, Ti₇₀Si₃₀, Ti₅₀Si₅₀, Ti₄₀Si₆₀, and TiO₂SiO₂ exhibited higher weight loss as a function of immersion time than neat PLA. In this case, TiO₂, SiO₂, Ti₇₀Si₃₀, Ti₅₀Si₅₀, Ti₄₀Si₆₀, and TiO₂SiO₂ dispersed in the PLA matrix, the water molecules penetrated easier

within the samples to generate the degradation process and might have been absorbed into the gap between the conglomeration of the nanoparticles due to the agglomeration of the nanofiller. Consequently, a long time is spent on diffusion into the PLA matrix. Therefore, the degradation rate increased in the first period and reached its maximum [62]. In addition, the mass loss of the PLA composite was also found to increase with an increasing amount of $Ti_{70}Si_{30}$ to 5 wt.%. Consequently, it could be concluded that the rate of the long-term degradation of the PLA composite films depended upon the content of the mixed oxide loading. This result was connected to the hydrophilicity of TiO_2 , SiO_2 , $Ti_{70}Si_{30}$, $Ti_{50}Si_{50}$, $Ti_{40}Si_{60}$, and TiO_2SiO_2 , as well as the high-water absorption of the composites [63]. Regarding changes in the tensile strength, elongation at the break and Young's modulus of the PLA and PLA composite films are shown in Table 5. This table shows that the tensile strength and elongation at the break of the PLA and all of the PLA composite films decreased significantly after 28 days of in vitro degradation. The result suggests that the PLA and PLA composite films were mechanically stable during 28 days of in vitro degradation. The tensile strengths of the PLA and PLA composites decreased after 28 days of degradation with microcracks appearing on part of their surfaces. It was supposed that the PLA composites would lose their mechanical strengths quickly after the microcracks developed over the whole area of the fibers [64].

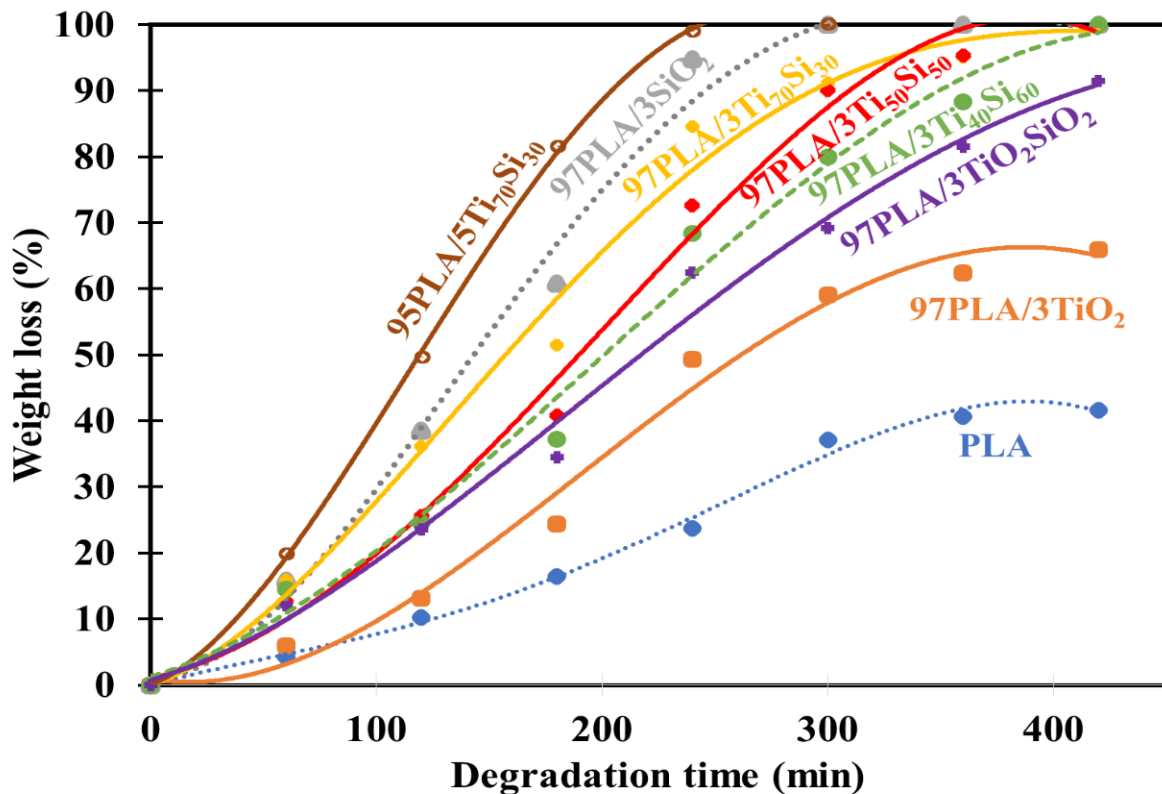


Figure 10. Weight loss of hydrolytic degradation of PLA, PLA/ TiO_2 , PLA/ SiO_2 , and PLA/ Ti_xSi_y composite films as functions of degradation time.

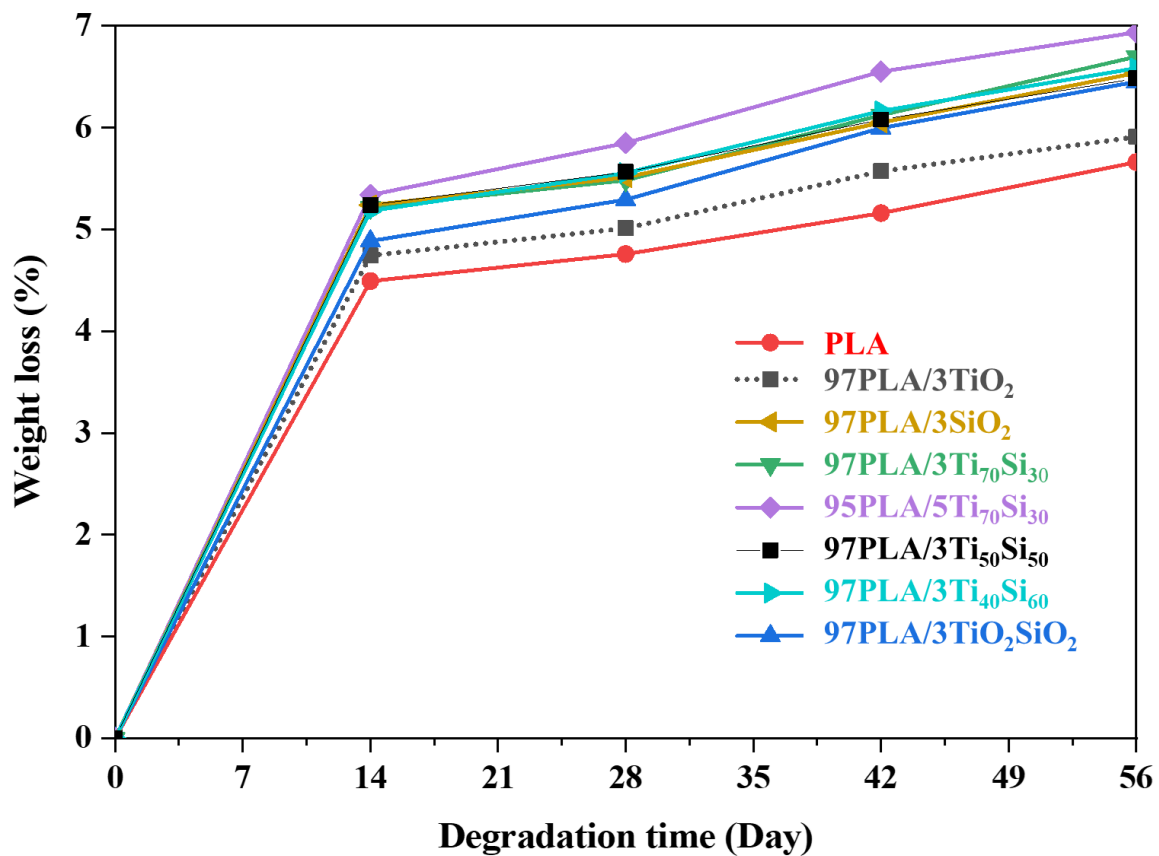


Figure 11. Weight loss of PLA, PLA/TiO₂, PLA/SiO₂, PLA/Ti_xSi_y, and PLA/TiO₂SiO₂ composites films after different periods of in vitro degradation.

Table 5. Tensile properties of properties of PLA, PLA/TiO₂, PLA/SiO₂, and PLA/Ti_xSi_y composite films after different period of in vitro degradation.

Time (Day)	Sample	Tensile Strength (MPa)	Elongation at Break (%)	Young's Modulus (GPa)
0	PLA	33.94 ± 1.38	19.62 ± 8.64	0.98 ± 0.23
	97PLA/3TiO ₂	28.22 ± 1.47	18.1 ± 4.24	1.01 ± 0.04
	97PLA/3SiO ₂	29.75 ± 1.38	11.8 ± 4.96	1.07 ± 0.10
	97PLA/3Ti ₇₀ Si ₃₀	35.64 ± 3.21	11.12 ± 1.81	1.18 ± 0.06
	95PLA/5Ti ₇₀ Si ₃₀	32.06 ± 2.29	9.88 ± 2.81	1.01 ± 0.10
	97PLA/3Ti ₅₀ Si ₅₀	35.31 ± 2.01	9.61 ± 2.57	1.29 ± 0.12
	97PLA/3Ti ₄₀ Si ₆₀	30.67 ± 1.74	22.30 ± 2.53	1.02 ± 0.05
	97PLA/3TiO ₂ SiO ₂	29.00 ± 1.42	58.37 ± 5.00	0.96 ± 0.07
14	PLA	29.43 ± 3.02	3.81 ± 1.61	1.51 ± 0.14
	97PLA/3TiO ₂	23.05 ± 2.87	2.58 ± 0.54	1.46 ± 0.31
	97PLA/3SiO ₂	23.53 ± 2.07	2.78 ± 0.27	1.39 ± 0.40
	97PLA/3Ti ₇₀ Si ₃₀	33.56 ± 3.45	3.69 ± 0.61	1.74 ± 0.14
	95PLA/5Ti ₇₀ Si ₃₀	31.75 ± 2.31	3.55 ± 0.70	1.49 ± 0.03
	97PLA/3Ti ₅₀ Si ₅₀	30.75 ± 2.51	3.45 ± 0.80	1.29 ± 0.04
	97PLA/3Ti ₄₀ Si ₆₀	27.99 ± 1.18	4.46 ± 0.95	1.21 ± 0.44
	97PLA/3TiO ₂ SiO ₂	24.83 ± 2.35	3.25 ± 0.38	1.44 ± 0.56

Table 5. Cont.

Time (Day)	Sample	Tensile Strength (MPa)	Elongation at Break (%)	Young's Modulus (GPa)
28	PLA	19.95 ± 2.45	2.06 ± 0.38	1.75 ± 0.25
	97PLA/3TiO ₂	18.69 ± 2.02	1.98 ± 0.23	2.02 ± 0.00
	97PLA/3SiO ₂	n/a *	n/a	n/a
	97PLA/3Ti ₇₀ Si ₃₀	29.35 ± 2.07	2.56 ± 0.12	1.91 ± 0.39
	95PLA/5Ti ₇₀ Si ₃₀	10.03 ± 2.40	1.11 ± 0.33	n/a
	97PLA/3Ti ₅₀ Si ₅₀	18.03 ± 2.80	2.11 ± 0.23	n/a
	97PLA/3Ti ₄₀ Si ₆₀	17.56 ± 2.01	2.08 ± 0.13	n/a
	97PLA/3TiO ₂ SiO ₂	17.39 ± 2.46	1.79 ± 0.35	n/a
42	PLA	6.95 ± 2.49	1.33 ± 0.19	n/a
	97PLA/3TiO ₂	0.26 ± 0.11	0.81 ± 0.10	n/a
	97PLA/3SiO ₂	n/a	n/a	n/a
	97PLA/3Ti ₇₀ Si ₃₀	15.97 ± 2.62	1.52 ± 0.11	n/a
	95PLA/5Ti ₇₀ Si ₃₀	n/a	n/a	n/a
	97PLA/3Ti ₅₀ Si ₅₀	5.97 ± 2.63	0.62 ± 0.52	n/a
	97PLA/3Ti ₄₀ Si ₆₀	n/a	n/a	n/a
	97PLA/3TiO ₂ SiO ₂	3.24 ± 1.79	1.12 ± 0.64	n/a

* n/a = not available.

3.9. Antimicrobial Activity

Metal oxides hold greater antibacterial efficiency, and their reinforcement in polymer composites expressively expands the antimicrobial properties of the film, which is desired in biomedical and food packaging applications. Bacteria are generally characterized by the cell membrane, which is composed mostly of a homogeneous peptidoglycan layer (which consists of amino acids and sugar). Gram-positive bacteria such as *Staphylococcus aureus* have one cytoplasm membrane with multilayers of the peptidoglycan polymer and a thicker cell wall (20–80 nm) [65], whereas in Gram-negative bacteria such as *Escherichia coli*, the bacteria wall is composed of two cell membranes, and an outer membrane and a plasma membrane with a thin layer of peptidoglycan with a thickness of 7–8 nm [65].

TiO₂ nanoparticles are known for their antibacterial activity, and recent studies have confirmed their efficiency as antibacterial agents [65,66]. As a result, the antibacterial activity of PLA incorporated with 3 wt.% of Ti₇₀Si₃₀, Ti₅₀Si₅₀, and TiO₂SiO₂, and 5 wt.% of Ti₇₀Si₃₀, to form composites was compared to the antibacterial activity of PLA adding 3 wt.% of TiO₂. The results of the antimicrobial activity of the Gram-negative bacteria (*Escherichia coli* or *E. coli*) and Gram-positive bacteria (*Staphylococcus aureus* or *S. aureus*) of the PLA and PLA composites are shown in Tables 6 and 7, respectively. The number of bacteria *Escherichia coli* and bacteria *Staphylococcus aureus* on the PLA and PLA composite films at time 0 h (at dilution 10⁻³) and 24 h (at dilution 10⁰) are shown in Figure 12.

Table 6. Antimicrobial activity of Gram-negative bacteria (*Escherichia coli*) of PLA, PLA/TiO₂, PLA/Ti_xSi_y, and PLA/TiO₂SiO₂ composites.

Samples	Blank (Ut) (t = 24 h)	Sample (At) (t = 24 h)	Antimicrobial Activity ^a (R)
	Log CFU/mL	Log CFU/mL	
PLA	5.96 ± 0.01	5.87 ± 0.02	0.09
97PLA/3TiO ₂	5.96 ± 0.01	0.00 ± 0.00	5.96
97PLA/3Ti ₇₀ Si ₃₀	5.96 ± 0.01	0.00 ± 0.00	5.96
95PLA/5Ti ₇₀ Si ₃₀	5.96 ± 0.01	0.00 ± 0.00	5.96
97PLA/3Ti ₅₀ Si ₅₀	5.96 ± 0.01	3.21 ± 0.04	2.75
97PLA/3TiO ₂ SiO ₂	5.96 ± 0.01	2.53 ± 0.04	3.43

^a Antibacterial activity (R) ≥ 2 = antimicrobial effectiveness.

Table 7. Antimicrobial activity of Gram-positive bacteria (*Staphylococcus aureus*) of PLA, PLA/TiO₂, PLA/Ti_xSi_y, and PLA/TiO₂SiO₂ composites.

Samples	Blank (Ut) (t = 24 h)	Sample (At) (t = 24 h)	Antimicrobial Activity ^a (R)
	Log CFU/mL	Log CFU/mL	
PLA	4.35 ± 0.04	4.35 ± 0.04	0
PLA/3TiO ₂	4.35 ± 0.04	0.00 ± 0.00	4.35
PLA/3Ti ₇₀ Si ₃₀	4.35 ± 0.04	2.96 ± 0.01	2.04
PLA/5Ti ₇₀ Si ₃₀	4.35 ± 0.04	0.00 ± 0.00	4.35
PLA/3Ti ₅₀ Si ₅₀	4.35 ± 0.04	3.17 ± 0.08	1.83
PLA/3TiO ₂ SiO ₂	4.35 ± 0.04	3.21 ± 0.01	1.79

^a Antibacterial activity (R) ≥ 2 = antimicrobial effectiveness.

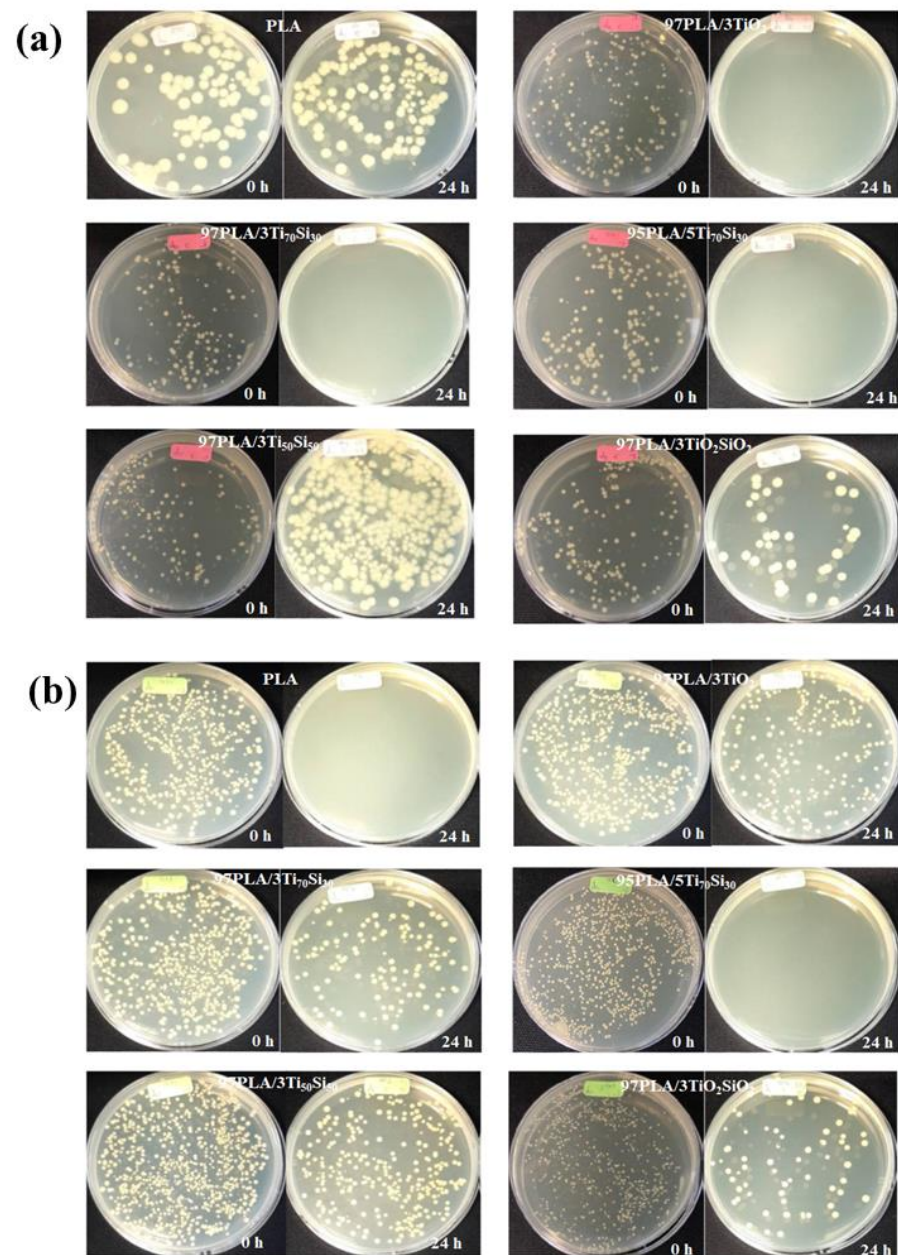


Figure 12. The number of (a) bacteria *Escherichia coli* and (b) bacteria *Staphylococcus aureus* on PLA and PLA composite films at time 0 h (at dilution 10⁻³) and 24 h (at dilution 10⁰).

The antimicrobial activity (R) values of Neat PLA film against *E. coli* and *S. aureus* were 0.09 and 0, respectively. This result shows that PLA has no significant antibacterial effects on *E. coli* and *S. aureus*. However, the 97PLA/3TiO₂ composite film exhibited the highest antimicrobial activity (R = 5.96 against *E. coli* and R = 4.35 against *S. aureus*). As shown in Table 6, all of PLA composites exhibited an antimicrobial activity agent against *E. coli* (if $R \geq 2$ antimicrobial effectiveness). Moreover, the results confirm that PLA incorporated with 3wt.% of Ti₇₀Si₃₀ has sufficient antimicrobial effectiveness. Likewise, PLA with the addition of 3 wt.% of TiO₂ and Ti₇₀Si₃₀ exhibited an antibacterial effect on *S. aureus*. This was due to TiO₂ and Ti_xSi_y oxide utilizing a similar mechanism against bacterial growth by directly damaging the bacterial surface. Adding TiO₂ and Ti_xSi_y oxide into PLA could lead to reduced soluble protein expression by suppressing the synthesis of nucleic acids. Thus, TiO₂ and Ti_xSi_y oxide antibacterial action against *S. aureus* was probably through inhibiting the synthesis of nucleic acid, thereby reducing protein synthesis against bacterial growth [67]. The mechanism referred to as the antimicrobial action of TiO₂ is commonly associated with reactive oxygen species (ROS) with high oxidative potentials produced under a band-gap irradiation photo-induced charge in the presence of O₂ [68]. Pleskova et al. investigated the bactericidal activity of the TiO₂ film and discovered that *S. aureus* is swelled by TiO₂ through damaging the cell membrane [69]. In addition, the increase of Ti₇₀Si₃₀ loading to 5 wt.% improved the antimicrobial effectiveness of the PLA composites. However, 97PLA/3Ti₅₀Si₅₀ and 97PLA/3TiO₂SiO₂ exhibited low antimicrobial activity (R = 2.75, 3.43 against *E. coli* and R = 1.83, 1.79 against *S. aureus*). This was due to a higher SiO₂ content in Ti₅₀Si₅₀ and TiO₂SiO₂, resulting in a lower efficiency of antimicrobial activity. In addition, the variation in the microorganism structure between the Gram-negative (*E. coli*) and Gram-positive (*S. aureus*) bacteria may explain the difference in the antibacterial effect of samples against *E. coli* and *S. aureus*. Both bacteria have similar internal, but different external structures. The peptidoglycan layer of Gram-positive bacteria is thick and includes teichoic and lipoteichoic acids. A Gram-negative bacterium has a thin peptidoglycan layer and an outer membrane made up of proteins, phospholipids, and lipopolysaccharides. Therefore, *S. aureus* needs longer contact time or higher catalyst concentrations to achieve the same effect as *E. coli* [70].

4. Conclusions

The aim of this study was to examine the influence of 3wt.% of TiO₂, SiO₂, Ti₇₀Si₃₀, Ti₅₀Si₅₀, Ti₄₀Si₆₀, and TiO₂SiO₂, and 5 wt.% of Ti₇₀Si₃₀ on the mechanical properties, thermal properties, morphological properties, degradation behavior, and antimicrobial activity of PLA. The PLA and PLA composites films were obtained by the solvent casting method. The addition of Ti₇₀Si₃₀ and Ti₅₀Si₅₀ into the PLA film slightly improved the tensile strength and Young's modulus of PLA. The incorporation of 5 wt.% of Ti₇₀Si₃₀ was found to decrease the cold crystallization temperature and increased the degree of crystallinity of PLA. It can be concluded that Ti₇₀Si₃₀ nanoparticles can act as a good nucleating agents for PLA. The thermal stability of PLA was enhanced with the incorporation of TiO₂ and SiO₂. The water vapor transmission rate (WVTR) of PLA was significantly increased by the incorporation of SiO₂, Ti₇₀Si₃₀, and Ti₅₀Si₅₀ nanoparticles. This is due to the hydrophilicity of the nanoparticles. In addition, efficiency of degrading MB is TiO₂ > Ti₇₀Si₃₀ > TiO₂SiO₂ > Ti₅₀Si₅₀ > Ti₄₀Si₆₀ > SiO₂, respectively. Moreover, the increase in Ti₇₀Si₃₀ loading to 5 wt.% improved the efficiency of the photocatalytic activity of PLA. All of the nanoparticles were able to remove UV light and, in particular, TiO₂ and Ti₇₀Si₃₀ enhanced a stronger higher UV-shielding potential. The hydrolytic degradation and in vitro degradation of PLA are important properties of the variety of application such as biomedical application and food packaging. PLA incorporated with 3wt.% of SiO₂, Ti₇₀Si₃₀, Ti₅₀Si₅₀, Ti₄₀Si₆₀, and TiO₂SiO₂ exhibited much higher weight loss as a function of time than neat PLA. The weight loss of the PLA composite was also found to increase with increasing Ti₇₀Si₃₀ to 5 wt.%. Furthermore, PLA with the addition of TiO₂ and Ti₇₀Si₃₀ exhibited an excellent

antibacterial effect on Gram-negative bacteria (*E. coli*) and Gram-positive bacteria (*S. aureus*), indicating the improved antimicrobial effectiveness of PLA composites.

Supplementary Materials: The following supporting information can be downloaded at: <https://www.mdpi.com/article/10.3390/polym14163310/s1>, Figure S1: Curve of (a) TGA thermogram, (b) DTG Thermogram of PLA, PLA/TiO₂, PLA/SiO₂, PLA/Ti_xSi_y, and PLA/TiO₂SiO₂ composites.; Figure S2: The changes in tensile properties of PLA, PLA/TiO₂, PLA/SiO₂, and PLA/Ti_xSi_y composite films after different periods of in vitro degradation.

Author Contributions: Conceptualization, Y.R.; methodology, A.T., C.R. and Y.R.; validation, A.T., C.R. and Y.R.; formal analysis, A.T.; investigation, A.T., C.R. and Y.R.; resources, A.T., C.R. and Y.R.; data curation, A.T.; writing—original draft preparation, A.T.; writing—review and editing, A.T., C.R. and Y.R.; visualization, C.R. and Y.R.; supervision, C.R. and Y.R.; project administration, C.R. and Y.R.; funding acquisition, C.R. and Y.R. All authors have read and agreed to the published version of the manuscript.

Funding: This research was funded by Thailand Science Research and Innovation (TSRI), grant number 42853.

Institutional Review Board Statement: Not applicable.

Informed Consent Statement: Not applicable.

Data Availability Statement: Not applicable.

Acknowledgments: The authors are grateful to Suranaree University of Technology (SUT); to the Center of Excellence on Petrochemical and Materials Technology (PETROMAT); to the Science, Research and Innovation Promotion Fund from Thailand Science Research and Innovation (TSRI); and to the Research Center for Biocomposite Materials for the Medical Industry and Agricultural and Food Industry for the financial support.

Conflicts of Interest: The authors declare no conflict of interest.

References

1. Cadar, O.; Paul, M.; Roman, C.; Miclean, M.; Majdik, C. Biodegradation behaviour of poly(lactic acid) and (lactic acid-ethylene glycol-malonic or succinic acid) copolymers under controlled composting conditions in a laboratory test system. *Polym. Degrad. Stab.* **2012**, *97*, 354–357. [[CrossRef](#)]
2. Lim, L.T.; Auras, R.; Rubino, M. Processing technologies for poly(lactic acid). *Prog. Polym. Sci.* **2008**, *33*, 820–852. [[CrossRef](#)]
3. Deroiné, M.; Le Duigou, A.; Corre, Y.M.; Le Gac, P.Y.; Davies, P.; César, G.; Bruzard, S. Accelerated ageing of polylactide in aqueous environments: Comparative study between distilled water and seawater. *Polym. Degrad. Stab.* **2014**, *108*, 319–329. [[CrossRef](#)]
4. Wang, Y.; Kong, Y.; Zhao, Y.; Feng, Q.; Wu, Y.; Tang, X.; Gu, X.; Yang, Y. Electrospun, reinforcing network-containing, silk fibroin-based nerve guidance conduits for peripheral nerve repair. *J. Biomater. Tissue Eng.* **2016**, *6*, 53–60. [[CrossRef](#)]
5. Athanasiou, K.A.; Niederauer, G.G.; Agrawal, C.M. Sterilization, toxicity, biocompatibility and clinical applications of polylactic acid/polyglycolic acid copolymers. *Biomaterials* **1996**, *17*, 93–102. [[CrossRef](#)]
6. Cheung, H.Y.; Lau, K.T. Study on a silkworm silk fiber/biodegradable polymer biocomposite. In Proceedings of the ICCM International Conferences on Composite Materials, Kyoto, Japan, 8–13 July 2007.
7. Yeh, J.T.; Huang, C.Y.; Chai, W.L.; Chen, K.N. Plasticized properties of poly (lactic acid) and triacetin blends. *J. Appl. Polym. Sci.* **2009**, *112*, 2757–2763. [[CrossRef](#)]
8. Burg, K.J.L.; Holder, W.D.; Culberson, C.R.; Beiler, R.J.; Greene, K.G.; Loebbeck, A.B.; Roland, W.D.; Mooney, D.J.; Halberstadt, C.R. Parameters affecting cellular adhesion to polylactide films. *J. Biomater. Sci. Polym. Ed.* **1999**, *10*, 147–161. [[CrossRef](#)]
9. Rasal, R.M.; Janorkar, A.V.; Hirt, D.E. Poly(lactic acid) modifications. *Prog. Polym. Sci.* **2010**, *35*, 338–356. [[CrossRef](#)]
10. Paul, M.A.; Delcourt, C.; Alexandre, M.; Degée, P.; Monteverde, F.; Dubois, P. Polylactide/montmorillonite nanocomposites: Study of the hydrolytic degradation. *Polym. Degrad. Stab.* **2005**, *87*, 535–542. [[CrossRef](#)]
11. Shogren, R.L.; Doane, W.M.; Garlotta, D.; Lawton, J.W.; Willett, J.L. Biodegradation of starch/polylactic acid/poly(hydroxyester-ether) composite bars in soil. *Polym. Degrad. Stab.* **2003**, *79*, 405–411. [[CrossRef](#)]
12. Buzarovska, A.; Grozdanov, A. Biodegradable poly(L-lactic acid)/TiO₂ nanocomposites: Thermal properties and degradation. *J. Appl. Polym. Sci.* **2012**, *123*, 2187–2193. [[CrossRef](#)]
13. Yang, K.K.; Wang, X.L.; Wang, Y.Z. Progress in nanocomposite of biodegradable polymer. *J. Ind. Eng. Chem.* **2007**, *13*, 485–500.
14. Huang, S.M.; Hwang, J.J.; Liu, H.J.; Lin, L.H. Crystallization behavior of poly(L-lactic acid)/montmorillonite nanocomposites. *J. Appl. Polym. Sci.* **2010**, *117*, 434–442. [[CrossRef](#)]

15. Tang, H.; Chen, J.B.; Wang, Y.; Xu, J.Z.; Hsiao, B.S.; Zhong, G.J.; Li, Z.M. Shear flow and carbon nanotubes synergistically Induced nonisothermal crystallization of poly(lactic acid) and its application in injection molding. *Biomacromolecules* **2012**, *13*, 3858–3867. [[CrossRef](#)]
16. Murariu, M.; Paint, Y.; Murariu, O.; Raquez, J.-M.; Bonnaud, L.; Dubois, P. Current progress in the production of PLA–ZnO nanocomposites: Beneficial effects of chain extender addition on key properties. *J. Appl. Polym. Sci.* **2015**, *132*, 42480. [[CrossRef](#)]
17. Hakim, R.H.; Cailloux, J.; Santana, O.O.; Bou, J.; Sánchez-Soto, M.; Odent, J.; Raquez, J.M.; Dubois, P.; Carrasco, F.; MasPOCH, M.L. PLA/SiO₂ composites: Influence of the filler modifications on the morphology, crystallization behavior, and mechanical properties. *J. Appl. Polym. Sci.* **2017**, *134*, 45367. [[CrossRef](#)]
18. Wu, G.; Liu, S.; Jia, H.; Dai, J. Preparation and properties of heat resistant polylactic acid (PLA)/Nano-SiO₂ composite filament. *J. Wuhan Univ. Technol. Mater. Sci. Ed.* **2016**, *31*, 164–171. [[CrossRef](#)]
19. Xiu, H.; Qi, X.; Bai, H.; Zhang, Q.; Fu, Q. Simultaneously improving toughness and UV-resistance of polylactide/titanium dioxide nanocomposites by adding poly(ether)urethane. *Polym. Degrad. Stab.* **2017**, *143*, 136–144. [[CrossRef](#)]
20. Zapata, P.A.; Palza, H.; Cruz, L.S.; Lieberwirth, I.; Catalina, F.; Corrales, T.; Rabagliati, F.M. Polyethylene and poly(ethylene-co-1-octadecene) composites with TiO₂ based nanoparticles by metallocenic “in situ” polymerization. *Polymer* **2013**, *54*, 2690–2698. [[CrossRef](#)]
21. Fonseca, C.; Ochoa, A.; Ulloa, M.T.; Alvarez, E.; Canales, D.; Zapata, P.A. Poly(lactic acid)/TiO₂ nanocomposites as alternative biocidal and antifungal materials. *Mater. Sci. Eng. C* **2015**, *57*, 314–320. [[CrossRef](#)]
22. Wu, F.; Lan, X.; Ji, D.; Liu, Z.; Yang, W.; Yang, M. Grafting polymerization of polylactic acid on the surface of nano-SiO₂ and properties of PLA/PLA-grafted-SiO₂ nanocomposites. *J. Appl. Polym. Sci.* **2013**, *129*, 3019–3027. [[CrossRef](#)]
23. Serenko, O.A.; Muzafarov, A.M. Polymer composites with surface modified SiO₂ nanoparticles: Structures, properties, and promising applications. *Polym. Sci. Ser. C* **2016**, *58*, 93–101. [[CrossRef](#)]
24. Ha, S.W.; Weitzmann, M.N.; Beck, G.R., Jr. Applications of silica-based nanomaterials in dental and skeletal biology. In *Nanobiomaterials in Clinical Dentistry*; Karthikeyan, W., Ahmed, J.K., Eds.; Elsevier: Amsterdam, The Netherlands, 2013; pp. 69–91.
25. Galindo, I.R.; Viveros, T.; Chadwick, D. Synthesis and characterization of titania-based ternary and binary mixed oxides prepared by the sol–gel method and their activity in 2-propanol dehydration. *Ind. Eng. Chem. Res.* **2007**, *46*, 1138–1147. [[CrossRef](#)]
26. Liao, S.Y.; Read, D.C.; Pugh, W.J.; Furr, J.; Russell, A.D. Interaction of silver nitrate with readily identifiable groups: Relationship to the antibacterial action of silver ions. *Lett. Appl. Microbiol.* **1997**, *25*, 279–283. [[CrossRef](#)]
27. Marra, A.; Silvestre, C.; Duraccio, D.; Cimmino, S. Polylactic acid/zinc oxide biocomposite films for food packaging application. *Int. J. Biol. Macromol.* **2016**, *88*, 254–262. [[CrossRef](#)]
28. Sirelkhatim, A.; Mahmud, S.; Seeni, A.; Kaus, N.H.M.; Ann, L.C.; Bakhori, S.K.M.; Hasan, H.; Mohamad, D. Review on zinc oxide nanoparticles: Antibacterial activity and toxicity mechanism. *Nano-Micro Lett.* **2015**, *7*, 219–242. [[CrossRef](#)]
29. Li, W.; Zhang, C.; Chi, H.; Li, L.; Lan, T.; Han, P.; Chen, H.; Qin, Y. Development of antimicrobial packaging film made from poly(lactic acid) incorporating titanium dioxide and silver nanoparticles. *Molecules* **2017**, *22*, 1170. [[CrossRef](#)]
30. Shebi, A.; Lisa, S. Evaluation of biocompatibility and bactericidal activity of hierarchically porous PLA-TiO₂ nanocomposite films fabricated by breath-figure method. *Mater. Chem. Phys.* **2019**, *230*, 308–318. [[CrossRef](#)]
31. Swaroop, C.; Shukla, M. Polylactic acid/magnesium oxide nanocomposite films for food packaging applications. In Proceedings of the 21st International Conference on Composite Materials, Xi’an, China, 20–25 August 2017.
32. Teamsinsungvon, A.; Sutapun, W.; Ruksakulpiwat, C.; Ruksakulpiwat, Y. Preparation of titanium-silica binary mixed oxide to use as a filler in poly (lactic acid). *Suranaree J. Sci. Technol.* **2019**, *26*, 31–36.
33. Teamsinsungvon, A.; Ruksakulpiwat, C.; Amonpattaratkit, P.; Ruksakulpiwat, Y. Structural Characterization of Titanium–Silica Oxide Using Synchrotron Radiation X-ray Absorption Spectroscopy. *Polymers* **2022**, *14*, 2729. [[CrossRef](#)]
34. Matijević, E.; Budnik, M.; Meites, L. Preparation and mechanism of formation of titanium dioxide hydrosols of narrow size distribution. *J. Colloid Interface Sci.* **1977**, *61*, 302–311. [[CrossRef](#)]
35. Vorkapic, D.; Matsoukas, T. Effect of Temperature and Alcohols in the Preparation of Titania Nanoparticles from Alkoxides. *J. Am. Ceram. Soc.* **1998**, *81*, 2815–2820. [[CrossRef](#)]
36. Cheung, H.Y.; Lau, K.T.; Tao, X.M.; Hui, D. A potential material for tissue engineering: Silkworm silk/PLA biocomposite. *Compos. Part B Eng.* **2008**, *39*, 1026–1033. [[CrossRef](#)]
37. Boonying, S.; Sutapun, W.; Suppakarn, N.; Ruksakulpiwat, Y. Crystallization Behavior of Vetiver Grass Fiber-Polylactic Acid Composite. *Adv. Mater. Res.* **2012**, *410*, 55–58. [[CrossRef](#)]
38. Tang, Z.; Zhang, C.; Liu, X.; Zhu, J. The crystallization behavior and mechanical properties of polylactic acid in the presence of a crystal nucleating agent. *J. Appl. Polym. Sci.* **2012**, *125*, 1108–1115. [[CrossRef](#)]
39. Elsner, J.; Shefy-Peleg, A.; Zilberman, M. Novel biodegradable composite wound dressings with controlled release of antibiotics: Microstructure, mechanical and physical properties. *J. Biomed. Mater. Res. Part B Appl. Biomater.* **2010**, *93*, 425–435. [[CrossRef](#)]
40. Teo, P.S.; Chow, W.S. Water vapour permeability of poly(lactic acid)/chitosan binary and ternary blends. *Appl. Sci. Eng. Prog.* **2014**, *7*, 23–27.
41. Feng, S.; Zhang, F.; Ahmed, S.; Liu, Y. Physico-mechanical and antibacterial properties of PLA/TiO₂ composite materials synthesized via electrospinning and solution casting processes. *Coatings* **2019**, *9*, 525. [[CrossRef](#)]

42. Felfel, R.M.; Leander, P.; Miquel, G.F.; Tobias, M.; Gerhard, H.; Ifty, A.; Colin, S.; Virginie, S.; David, M.G.; Klaus, L. In vitro degradation and mechanical properties of PLA-PCL copolymer unit cell scaffolds generated by two-photon polymerization. *Biomed. Mater.* **2016**, *11*, 015011. [[CrossRef](#)]
43. Racksanti, A.; Janhom, S.; Punyanitya, S.; Watanesk, R.; Watanesk, S. An approach for preparing an absorbable porous film of silk fibroin–rice starch modified with trisodium trimetaphosphate. *J. Appl. Polym. Sci.* **2015**, *132*, 41517. [[CrossRef](#)]
44. Sarasua, J.R.; Prud'homme, R.E.; Wisniewski, M.; Le Borgne, A.; Spassky, N. Crystallization and melting behavior of polylactides. *Macromolecules* **1998**, *31*, 3895–3905. [[CrossRef](#)]
45. Chen, P.; Zhou, H.; Liu, W.; Zhang, M.; Du, Z.; Wang, X. The synergistic effect of zinc oxide and phenylphosphonic acid zinc salt on the crystallization behavior of poly (lactic acid). *Polym. Degrad. Stab.* **2015**, *122*, 25–35. [[CrossRef](#)]
46. Chen, R.Y.; Zou, W.; Wu, C.R.; Jia, S.K.; Huang, Z.; Zhang, G.Z.; Yang, Z.T.; Qu, J.P. Poly(lactic acid)/poly(butylene succinate)/calcium sulfate whiskers biodegradable blends prepared by vane extruder: Analysis of mechanical properties, morphology, and crystallization behavior. *Polym. Test.* **2014**, *34*, 1–9. [[CrossRef](#)]
47. Zhang, H.; Huang, J.; Yang, L.; Chen, R.; Zou, W.; Lin, X.; Qu, J. Preparation, characterization and properties of PLA/TiO₂ nanocomposites based on a novel vane extruder. *RSC Adv.* **2015**, *5*, 4639–4647. [[CrossRef](#)]
48. Buzarovska, A. PLA nanocomposites with functionalized TiO₂ nanoparticles. *Polym. Plast. Technol. Eng.* **2013**, *52*, 280–286. [[CrossRef](#)]
49. Garlotta, D.; Doane, W.; Shogren, R.; Lawton, J.; Willett, J.L. Mechanical and thermal properties of starch-filled poly(D,L-lactic acid)/poly(hydroxy ester ether) biodegradable blends. *J. Appl. Polym. Sci.* **2003**, *88*, 1775–1786. [[CrossRef](#)]
50. Yew, G.H.; Mohd Yusof, A.M.; Mohd Ishak, Z.A.; Ishiaku, U.S. Water absorption and enzymatic degradation of poly(lactic acid)/rice starch composites. *Polym. Degrad. Stab.* **2005**, *90*, 488–500. [[CrossRef](#)]
51. Hu, Y.; Topolkarayev, V.; Hiltner, A.; Baer, E. Measurement of water vapor transmission rate in highly permeable films. *J. Appl. Polym. Sci.* **2001**, *81*, 1624–1633. [[CrossRef](#)]
52. Choudalakis, G.; Gotsis, A.D. Permeability of polymer/clay nanocomposites: A review. *Eur. Polym. J.* **2009**, *45*, 967–984. [[CrossRef](#)]
53. Tantekin-Ersolmaz, Ş.B.; Atalay-Oral, Ç.; Tatlier, M.; Erdem-Şenatalar, A.; Schoeman, B.; Sterte, J. Effect of zeolite particle size on the performance of polymer–zeolite mixed matrix membranes. *J. Membr. Sci.* **2000**, *175*, 285–288. [[CrossRef](#)]
54. Chen, L.; Zheng, K.; Liu, Y. Geopolymer-supported photocatalytic TiO₂ film: Preparation and characterization. *Constr. Build. Mater.* **2017**, *151*, 63–70. [[CrossRef](#)]
55. Zhuang, J.; Zhang, B.; Wang, Q.; Guan, S.; Li, B. Construction of novel ZnTiO₃/g-C₃N₄ heterostructures with enhanced visible light photocatalytic activity for dye wastewater treatment. *J. Mater. Sci. Mater. Electron.* **2019**, *30*, 6322–6334. [[CrossRef](#)]
56. Wang, Q.; Zhang, L.; Guo, Y.; Shen, M.; Wang, M.; Li, B.; Shi, J. Multifunctional 2D porous g-C₃N₄ nanosheets hybridized with 3D hierarchical TiO₂ microflowers for selective dye adsorption, antibiotic degradation and CO₂ reduction. *Chem. Eng. J.* **2020**, *396*, 125347. [[CrossRef](#)]
57. Asmatulu, R.; Mahmud, G.A.; Hille, C.; Misak, H.E. Effects of UV degradation on surface hydrophobicity, crack, and thickness of MWCNT-based nanocomposite coatings. *Prog. Org. Coat.* **2011**, *72*, 553–561. [[CrossRef](#)]
58. Oleyaei, S.A.; Zahedi, Y.; Ghanbarzadeh, B.; Moayedi, A.A. Modification of physicochemical and thermal properties of starch films by incorporation of TiO₂ nanoparticles. *Int. J. Biol. Macromol.* **2016**, *89*, 256–264. [[CrossRef](#)] [[PubMed](#)]
59. Cui, R.; Jiang, K.; Yuan, M.; Cao, J.; Li, L.; Tang, Z.; Qin, Y. Antimicrobial film based on polylactic acid and carbon nanotube for controlled cinnamaldehyde release. *J. Mater. Res. Technol.* **2020**, *9*, 10130–10138. [[CrossRef](#)]
60. Chu, Z.; Zhao, T.; Li, L.; Fan, J.; Qin, Y. Characterization of Antimicrobial Poly (Lactic Acid)/Nano-Composite Films with Silver and Zinc Oxide Nanoparticles. *Materials* **2017**, *10*, 659. [[CrossRef](#)]
61. Sinha Ray, S.; Yamada, K.; Okamoto, M.; Ueda, K. Polylactide-layered silicate nanocomposite: a novel biodegradable material. *Nano Lett.* **2002**, *2*, 1093–1096. [[CrossRef](#)]
62. Luo, Y.B.; Wang, X.L.; Wang, Y.Z. Effect of TiO₂ nanoparticles on the long-term hydrolytic degradation behavior of PLA. *Polym. Degrad. Stab.* **2012**, *97*, 721–728. [[CrossRef](#)]
63. Kaseem, M.; Hamad, K.; Ur Rehman, Z. Review of recent advances in polylactic acid/TiO₂ Composites. *Materials* **2019**, *12*, 3659. [[CrossRef](#)]
64. Yuan, X.; Mak, A.F.T.; Yao, K. In vitro degradation of poly(L- lactic acid) fibers in phosphate buffered saline. *J. Appl. Polym. Sci.* **2002**, *85*, 936–943. [[CrossRef](#)]
65. Fu, G.; Vary, P.S.; Lin, C.T. Anatase TiO₂ nanocomposites for antimicrobial coatings. *J. Phys. Chem. B* **2005**, *109*, 8889–8898. [[CrossRef](#)]
66. Joost, U.; Juganson, K.; Visnapuu, M.; Mortimer, M.; Kahru, A.; Nõmmiste, E.; Joost, U.; Kisand, V.; Ivask, A. Photocatalytic antibacterial activity of nano-TiO₂ (anatase)-based thin films: Effects on *Escherichia coli* cells and fatty acids. *J. Photochem. Photobiol. B Biol.* **2015**, *142*, 178–185. [[CrossRef](#)]
67. Jiang, X.; Lv, B.; Wang, Y.; Shen, Q.; Wang, X. Bactericidal mechanisms and effector targets of TiO₂ and Ag-TiO₂ against *Staphylococcus aureus*. *J. Med. Microbiol.* **2017**, *66*, 440–446. [[CrossRef](#)] [[PubMed](#)]
68. Verdier, T.; Coutand, M.; Bertron, A.; Roques, C. Antibacterial Activity of TiO₂ Photocatalyst Alone or in Coatings on *E. coli*: The Influence of Methodological Aspects. *Coatings* **2014**, *4*, 670–686. [[CrossRef](#)]

-
69. Pleskova, S.N.; Golubeva, I.S.; Verevkin, Y.K. Bactericidal activity of titanium dioxide ultraviolet-induced films. *Mater. Sci. Eng. C* **2016**, *59*, 807–817. [[CrossRef](#)] [[PubMed](#)]
 70. Talebian, N.; Zare, E. Structure and antibacterial property of nano-SiO₂ supported oxide ceramic. *Ceram. Int.* **2014**, *40*, 281–287. [[CrossRef](#)]